Genetic Tuning of Iron Oxide Nanoparticle Size, Shape, and Surface Properties in Magnetospirillum magneticum

Genetic tuning of iron oxide nanoparticle size, shape and surface properties in *Magnetospirillum magneticum*

Maiko Furubayashi[1], Andrea K. Wallace[1], Lina M. González[1], Justin P. Jahnke[2], Brendan M. Hanrahan[2], Alexis L. Payne[2], Dimitra N. Stratis-Cullum[2], Matthew T. Gray[3], Han Liu[3], Melissa Rhoads[3], Christopher A Voigt[1*]

1. *Synthetic Biology Center, Department of Biological Engineering, Massachusetts Institute of Technology, Cambridge, MA 02139*

2. *CCDC Army Research Laboratory, Adelphi, MD, USA*

3. Lockheed Martin Corporation, 2323 Eastern Blvd, Baltimore, 21220

* Corresponding author. E-mail: cavoigt@gmail.com

Keywords: Synthetic biology, nanotechnology, inducible system, genetic parts, mineralization

Abstract

Different applications require iron oxide nanoparticles (IONPs) of varying size, shape, crystallinity, and surfaces that can be controlled through the synthesis reaction conditions. Under ambient conditions, *Magnetospirillum magneticum* AMB-1 builds uniform Fe_3O_4 IONPs with shapes and

crystal forms difficult to achieve with chemical synthesis. Genetic engineering can be used to change their properties, but there are few tools to fine-tune expression over a wide range. To this end, we have designed ribosome binding sites (RBSs), minimal constitutive promoters, and inducible systems (IPTG, aTc, and OC6) that have low background and large fold-induction. These are used to control *M. magneticum* genes that affect IONP properties, including size (*mamC*), morphology (*mms6*), chain length (*mamK*), and surface coating (*mamC* fusions). These systems increase the fraction of IONPs that are less than 30 nm, produce rounded particles, and lead to the production of intracellular chains with 24 or more IONPs. In addition, the R5 peptide sourced from diatoms is found to silica-coat the surface of metal oxide nanoparticles (Fe, Ti, Ta, Hf) and can be genetically directed to the surface of *Magnetospirillum* IONPs. This work demonstrates the genetic control of IONP properties, but also highlights the robustness of the system that complicates genetic engineering to produce radically different particles and structures.

Introduction

The structure of iron oxide nanoparticles (IONPs) dictate their magnetic and optical properties and can be tuned to meet application needs, including spintronics, nanoscale sensors, and shape-changing or tunable-diffraction "smart" materials.[1-7] Size impacts magnetic properties, where particles <130 nm are single-domain ferromagnets and <30 nm are superparamagnetic (induced by an external field).[7-15] Different shapes are appropriate for different applications, for example, large surface areas for catalysts and long chains for antennas.[2-3, 16-20] Crystal forms have different uses, such as magnetite (Fe_3O_4) for ferrofluids and maghemite (γ-Fe_2O_3) for data storage.[14] It is challenging to control these properties using chemical syntheses, which are based on a nucleation step followed by crystal growth that, if unchecked, lead to irregular sizes and morphologies.[2-3, 21] After synthesis, IONPs are usually coated by a lipid to prevent aggregation and oxidation and can be functionalized.[9-10, 12, 22-23] Another approach is to encapsulate the nanoparticle in silica (SiO_2) because it is bio-inert, insulating, and can control spacing between particles.[24-27] Increased control over particle properties requires more extreme conditions and processing steps.

Under ambient conditions, some bacteria produce magnetite IONPs with properties often superior to those obtained through chemical synthesis.[28-32] Size is controlled by membrane "nanoreactors" in which iron particles are nucleated (magnetosomes).[32-33] The crystals grow to

nearly-perfect single domains with different species producing various lattice forms and shapes, including those that are cubic-, rectangular-, or bullet-shaped.[30, 34] A strong magnet requires the alignment of the single-domain IONPs into chains that increase the dipole moment and anisotropy.[30] The crystal form and chain organization stabilizes the magnetic moment from each particle and endows the organism to achieve the strongest permanent magnetism at ambient temperature and with the fewest Fe atoms.[30] The magnetosome lipid coating can be preserved and embedded with proteins to functionalize the IONPs.[21, 35-37] Purified magnetosomes can be chemically modified, for instance, by encapsulatition with a silica shell.[27] Isolated magnetosome nanoparticles exhibit low biotoxicity[38] and are promising candidates for biomedical applications.

Magnetospirillum magneticum AMB-1 and *Magnetospirillum gryphiswaledense* MSR-1 are closely-related, well-studied species that make 5-10 member linear chains of ~50 nm cubo-octahedral nanoparticles.[29, 32-33] IONP biogenesis genes are clustered in the genomic magnetosome island (MAI) with the essential genes in the *mamAB* operon.[39-43] While not essential for particle formation, the *mamGFDC* and *mms6F* operons encode proteins that anchor in the magnetosome membrane and guide IONP shape, size, and reduce crystal defects in both strains.[42, 44-46] The most abundant of which are Mms6 and MamC[47-48] (the latter also called Mms13[48] or Mam12[49]), which are small and have acidic domains that bind specific Fe surfaces and oxidation states with high affinity.[50-53] Knocking out *mms6* results in smaller or elongated particles with stunted crystallization in both magnetospirilla strains.[42, 45, 54] When *mamC* is knocked out, there is a minor effect in *M. magneticum*,[55] but this leads to smaller particles in *M. gryphiswaldense.*[44] The IONP surface has been functionalized by fusing these proteins to fluorescent reporters, silk fibroins, human/viral epitopes, nanobodies, and organophosphate-degrading enzymes.[21, 36-37] The magnetosomes are organized into chains by MamK, an actin homologue that assembles into 100 μm bundles.[56-58]

Genetic tools have been developed to control gene expression in magnetospirilla. Broad-host-range plasmids are commonly used,[59] including pBBR, RK2 and RSF1010, and pMGT has been isolated from *M. magneticum* MGT-1.[59-60] Plasmid stability has been found to be an issue in *M. gryphiswaldense.*[61] Native constitutive promoters have been gleaned from the genome, of which the *mamDC* (in *M. gryphiswaldense*) and *mms16* (in *M. magneticum*) promoters have been reported to be strong.[61-63] Promoters from other species, such as *E. coli*, are often weak in magnetospirilla and inducible systems that are transferred often fail or perform poorly in *M. gryphiswaldense.*[61-62] High background is a problem, which has been addressed in *M. magneticum* by adding a riboswitch

or reducing copy number,[64] but these solutions also decrease maximum expression. An anhydrotetracycline (aTc)-inducible system has been built based on a native promoter and this results in low background and 10-fold induction.[61, 65] These genetic parts and inducible systems have used to elucidate the mechanisms of magnetosome biogenesis, control particle properties and genome engineering.[42, 44, 65-72]

Here, we present new methods to control gene expression in *M. magneticum* and apply them to control IONP structures. The commonly-used broad-host-range plasmids are unstable, but pMGT is stable for which we construct a minimal version. Expression levels are controlled using a set of constitutive promoters, including those based on a minimal *E. coli* architecture, and computationally-designed RBSs. Using these parts, three inducible systems are developed that respond to isopropyl β-d-1-thiogalactopyranoside (IPTG), aTc, and 3-oxohexanoyl-homoserine lactone (OC6) with low background activity and high maximal expression. To change the IONPs produced, these parts were applied to the overexpression of MamC, Mms6, MamK, and MamC-fusions. Increasing the expression of MamC produces graded control over particle size and shape and increases the number of particles in the superparamagnetic size regime. Mms6 over expression has little effect on size, but increase the abundance of smooth, spherical particles. MamK over expression increases the fraction of cells producing long (>15 particle) chains. Finally, the particles can be coated with silica shells by directing the SiO_2-condensing diatom R5 peptide to the surface with a MamC fusion.

Results

Production and purification of IONPs

We strived to identify conditions that lead to uniform particles with shapes that are reproducible in day-to-day experiments. *Magnetospirillum* are facultative microaerophilic bacteria with approximately 6 hour doubling time, and magnetosome production only occurs under specific media composition with limited range of redox potential and oxygen concentration.[73] Genomic stability can be a problem, particularly with respect to the loss of the MAI.[39] We found that routine variability in techniques, procedure and equipment could lead to different IONP titers and properties.

The first step was to increase the reliability of colony formation on agar plates (Figure 1a). Magnetospirilla are known to be sensitive on agar, particularly with respect to H_2O_2 accumulation, which can be scavenged by adding charcoal or catalase.[59, 74] However, we found this still leads to variability in colony formation, which we traced to charcoal-absorbing antibiotics[59] and unreliable catalase activity. We observed that using a different autoclave led to inconsistency in colony formation. Noting that H_2O_2 levels were due to autoclaving the phosphate salt with the agar,[75-76] we found that autoclaving the agar separately from the mMSGM media, and then mixing them just before making the plates, dramatically improved the number of colonies by more than six orders-of-magnitude (Figure 1b).

There were also problems encountered after colonies were picked from the plate into liquid culture and grown (Figure 1a). Our media initially included 35 mg/L ascorbic acid and 50 mg/L sodium thiosulfate as reducing agents, added before autoclaving.[74, 77] This led to variability in growth rate and magnetosome production (monitored as the "magnetic response" C_{mag}). However, if we added these reducing agents right before inoculation this inhibited growth, which we rectified by screening for reducing agents and concentrations (Supplementary Figure 1). Magnetosome formation is sensitive to redox potential and oxygen concentration.[73, 78] For this reason, ascorbic acid was used as a reducing agent to adjust the redox potential of the media. Some growth conditions also led to abundant polyhydroxyalkanoate (PHA) globules,[66] which we decreased by supplementing with additional $NaNO_3$ (Figure 1d and Supplementary Figure 2). Additional efforts to optimize conditions led to our development of a consolidated protocol (Supplemental Note 1), which resulted in stable growth and magnetism when passaged for 20 days (Figure 1c). Using this protocol, magnetosome production was scaled from 5 mL to 2 L and after growth for three days 1 mg/L of magnetosomes could be purified (Methods). The size and morphology of magnetosomes produced at different culture scales were indistinguishable.

Purifying high-quality magnetosomes also proved challenging (Figure 1a).[47, 79-82] We sought to maintain the magnetosome membrane after purification, but its association with cellular biomolecules increased cell debris. We found this was aided by the reduction of intracellular polyhydroxyalkanoate (PHA), use of a French press[80, 83] and implementing washing steps involving weak sonication and magnetic selection (Supplementary Figure 3; protocol described in Supplementary Note 1). Additional treatment removes the attached biomolecules, including alkaline buffer to remove surface-attached proteins which was first demonstrated for magnetosomes from

Magnetospirillum magnetotacticum MS-1[49] and sucrose-cushioned ultracentrifuge to separate magnetosomes used in magnetosomes isolated from *M. gryphiswaldense*.[47, 80] After purification, the magnetosomes can be observed by transmission electron microscopy (TEM) (Figures 1e/f, Supplementary Figures 3 and 4).

Stability of plasmid backbones

The broad-host-range pBBR1 and RSF1010 plasmids have been commonly used in *Magnetospirillum* strains.[59, 84] A cryptic plasmid (pMGT) was isolated from *M. magneticum* MGT-1 and reported to be stable in *M. magneticum* in the absence of selection.[60] We reconstructed a version of this plasmid through DNA synthesis and made more versatile versions with an origin of transfer (*oriT* from the RP4/RK2 plasmid) and origins of replications (ori's). The p15a and pUC ori's were added to make pMGA and pMGU, respectively. pMGB is a minimal version of pMGA with the *mob* gene removed. Various selection markers were tested (kanamycin and gentamicin) (Supplementary Figure 6). Experiments were designed to investigate and compare plasmid retention in *M. magneticum* by inserting a constitutive promoter (BBa_J23119) to drive the *sfgfp* reporter in the following plasmids: pBBR1, pRSF, pMGA and pMGB (Figure 1g). Cells were passaged over ten days in liquid media without antibiotics and plasmid loss was assayed by flow cytometry. After just 2 days, nearly all of the pBBR plasmid and a large fraction of pRSF was lost from the population, but pMGA and pMGB remained stable (Figure 1h,i).

Genetic parts to control expression in M. magneticum

We sought to build libraries of promoters and ribosome binding sites (RBSs) that could be used to tune gene expression. Noting that the constitutive promoter P_{tac} works efficiency in magnetospirilla,[77] we characterized five other commonly-used constitutive promoters[85] and the promoter from the kanamycin marker cassette, P_{neokan}. In addition, we designed four promoters based on the the *rrn* operon from *M. magneticum* (P_{rrn1}, P_{rrn1*}, P_{rrn4} and P_{rrn34}) (Supplementary Figure 7) and cloned four promoters from MAI or genome of magnetospirilla[61, 63] ($P_{mamDC45}$, P_{msp3}, P_{mms16} and P_{msp1}). Collectively, this yielded a set of 13 promoters (Table 1 and Supplementary Table S1).

To quantify their strength, the promoters were placed upstream of *sfgfp* in pMGA and the

fluorescence measured by flow cytometry (Figure 2a and Table 1) (Methods). The promoters derived from the MAI or genome were weak. Previously, $P_{mamDC45}$ was reported to be strong in *M. gryphiswaldense*[61-62] and this discrepancy could be due to species differences or a lack of a reference promoter in that work. In comparison, the P_{tac} and minimal promoters were 7- to 28-fold stronger. The strongest promoters were those based on the *rrn* architecture. The promoter strengths in *E. coli* and *M. magneticum* were only weakly correlated.

RBS sequences can be designed using the RBS Library Calculator, which creates degenerate sequences to maximize the range of expression levels across a set of RBSs based on a thermodynamic model to predict the translation initiation rates (TIRs).[86-88] Here, we used this software to design 16 RBS sequences using the 16S rRNA from *M. magneticum* (Table 1) (Methods). These sequences were placed downstream of a weak (BBa_J23117) and strong (BBa_J23119) constitutive promoter and the expression quantified (Figure 2b). RBS sequences predicted to have a higher TIR produce higher levels of expression over a 20-fold range.

Inducible systems

Genetic sensors that respond to small molecule inducers were designed using the genetic parts and pMGA plasmid. To prevent readthrough from regulator expression to their output promoter, the regulator gene is constitutively transcribed in the opposite orientation (Figure 2). The expression cassettes are insulated using the strong L3S2P21 terminator.[89] The RiboJ insulator is placed upstream of *sfgfp* because it has been shown to stabilize mRNA, resulting in increased expression.[90]

Three inducible systems were developed based on this architecture. First, we used a LacI variant ($LacI^{AM}$) (Q18M, A43V, F161Y) that has an improved dynamic range in *E. coli* and a P_{tac} promoter with two *lac* operators flanking it to reduce background (Supplementary Table 1).[91-92] In *M. magneticum*, this system showed a low basal level of activity close to background and generated a 22-fold induction (Figure 2c). The same approach was taken to build an aTc-inducible system based on TetR and P_{tet*} and this produced a 34-fold induction (Figure 2d). Of the three, this one produces the highest maximum expression. Quorum sensors are commonly used to program cell-cell communication and the chemical signal can be used as an inducer. LuxR is an activator that binds upstream of the -35 site to recruit RNA polymerase to the P_{lux} promoter. We used the LuxR/P_{lux} construct previously designed for *Rhizobia*,[93] which are in the same alphaproteobacteria class as *M.*

magneticum. This generated a 7-fold induction that is graded over a wide range of inducer levels (Figure 2e).

Control of IONP size and shape

It has been observed that changing the expression levels of MAI genes in magnetospirilla impacts the properties of the IONPs produced.[44-46, 71] This has been done by knocking out the gene or placing multiple copies of the gene under the control of a native MAI promoter. Knockouts have the potential to cause pleotropic phenotypes by affecting neighboring genes in the cluster. Therefore, we decided to leave the native gene intact while overexpressing a separate copy from a plasmid under inducible control.

First, we screened the MAI genes to determine which ones could impact the size or shape of the particles when highly expressed. Nine genes (*mamA, mamB, mamI, mamL, mamQ, mamR, mamS, mamT, mamV*) were cloned and placed under the control of the inducible variant of P_{tac} on pMGA. The RBS for each gene was designed using the RBS Calculator, selecting those that produce high translation rates that are about equal for each gene (Methods). The plasmids were conjugated into *M. magneticum* and the genes were fully induced with 1 mM IPTG for 48 hours. The magnetosomes were observed in cells using TEM (Supplementary Figures 8-9, 12-20). In three cases (*mamA, mamQ, mamL*), no differences were observed when compared to those produced by wild-type cells. Slight changes were observed when other genes were overexpressed (*mamR, mamI, mamV, mamB, mamT*), but we deemed them not interesting to pursue further. These results speak to the robustness of the system to the overexpression of most genes. The exception was the overexpression of *mamS*, which led to a large decrease in the number of magnetosomes per cell.

Next, the complete *mamGFDC* and *mms6F* operons were placed under the control of P_{tac} and the resulting particles were imaged when maximally induced (Supplementary Figures 10 and 11). In both cases, we observed a wide range of sizes and shapes, including cubic, round and those of small size. For the *mms6F*-expressing strain, we observed some magnetosomes with a rounded shape, which we rarely observed amongst those produced by the wild-type. Each of the six genes from these operons (*mamG, mamF, mamD, mamC, mms6* and *mmsF*) was cloned under P_{tac} control and RBSs were designed for each gene to achieve high and consistent expression. The plasmids were conjugated into *M. magneticum* and induced through the addition of 1-5 mM IPTG for 48 hours and

the magnetosomes imaged by TEM (Methods). In the *M. magneticum* strains expressing either *mamG*, *mamD* or *mms6,* there was an increased number of "round" magnetosome particles, which was most pronounced for *mms6* (Supplementary Figures 21-23). *mamF* or *mmsF* expression resulted in increase of the elongated rectangular particles (Supplementary Figures 24 and 25). In these strains, we also observed impaired or premature magnetosomes, suggesting these genes might be deleterious to the crystallization process. Finally, expressing *mamC* resulted in producing a mixture of particles, but all sharing symmetrical shape (circles and cubes, but not elongated ones) (Supplementary Figure 26). The overexpression of *mamC* showed less evidence of impaired or immature crystals, as compared to *mamF*/*mmsF*-expressing strains.

From the initial screens, we focused on two genes (*mamC* and *mms6*) for which there were uniform changes across mature crystals. Image processing software was used to analyze the size and shape of many particles (Methods). Using the IPTG-inducible system and constitutive promoters, the overexpression of *mamC* was found to reduce the size of the particles in a graded manner (Figure 3a,b). The shift of the size distribution (N = 150) shows that there is a large increase in the fraction of particles in the superparagnetic size range (<30 nm). When *mamC* is under the control of P_{rrn34}, 29% of the particles were in this range, compared to 6% for wild-type. Intermediate promoter strengths tune the fraction of particles that are small (Figure 3c).

We observed that the particles were rounder when *mamC* is expressed. Using image processing, we quantified a "shape factor" $(d_{min}/d_{max})^2$ of a particle where d_{min} and d_{max} are the minimum and the maximum Feret diameters, respectively. The maximum Feret diameter is the longest distance between any two points along the particle boundary and the minimum is the shortest possible distance. The *mamC*-magnetosomes showed increased shape factor compared to the wild-type (Figure 3d,e). This is consistent with work showing MamC *in vitro* produces particles with cube-like symmetry.[53] The overexpression of Mms6 had no effect on particle size, but produced a larger number of round particles at the highest levels of expression (Figure 3g-i). The less pronounced impact of Mms6 overexpression is consistent with *in vitro* studies, where MamC has been shown to have a more profound impact on crystal size.[50] We observed variability in the crystals, where some appear more similar to those produced by wild-type, which is consistent with evidence that Mms6 is only localized to a subset of magnetosomes.[94]

We characterized the physical properties of the IONPs produced by overexpressing MamC or Mms6 and compared them with those produced by wild-type cells (Supplementary Figure 31).

IONPs with their membranes intact (Supplementary Note 1) were harvested from cells containing P_{rrn34}-*mamC* or P_{tac}-*mms6* (with 1 mM IPTG). The quality of IONP purification was similar between samples, with Fourier-transform infrared spectroscopy (FTIR) indicating little cellular debris and X-ray photoelectron spectroscopy (XPS) consistent with an intact cellular membrane.[83] The XPS nitrogen (N) peak is higher for MamC, which may indicate a higher protein content in the membrane. The crystal form and oxidation state of all three samples is consistent with Fe_3O_4 (magnetite), as deduced by the peak locations and relative intensities measured by X-ray diffraction (XRD) (Powder Diffraction File (PDF) 98-008-5806) and the 2:1 ratio between XPS peaks associated with Fe p orbitals. The magnetization hysteresis was then measured for the samples, all three of which showed a characteristic loop for ferromagnetic material (Figure 3f,j). A sample of pure superparamagnetic particles would yield no hysteresis. The MamC sample has a larger fraction of particles in the superparamagnetic size range (29% versus 6% for wild-type) and this narrows the observed hysteresis (lower coercivity) (Figure 3f). The expression of Mms6 widened the hysteresis (increased coercivity) (Figure 3j). Given that the size, purity and crystal form of these IONPs are not different, this mostly like is due to the change in shape.

The overexpression of *mamK* leads to changes in the structure of the magnetosome chains (Figure 3k-m and Supplementary Figure 27). *mamK* was placed under the control of the IPTG-inducible P_{tac} promoter. When induced with IPTG, 12% of the cells have two adjacent chains of magnetosomes. This effect was not observed when expressing other MAI genes or under different culture conditions. Induction also leads to an enrichment in the presence of long magnetosome chains (>15) in the cell (Figure 3m).

Control of IONP surface properties

MamC has been used to anchor recombinant proteins to the magnetosome membrane.[61, 95-96] Using the IPTG-inducible system, we compared the *in vivo* expression of *sfgfp* with *mamC::sfgfp* and the *in vitro* expression of them after magnetosomes purification (Figure 4a). The cells expressing sfGFP showed bright fluorescence, while localized fluorescence was observed in the *mamC::sfgfp* cells, indicating the position of the magnetosomes within these cells. The stable plasmid ensures that all the cells in the culture population contains the plasmid and the purified magnetosomes uniformly display the surface peptide.

Diatoms are eukaryotic microorganisms that produce intricate silica structures.[97] During the formation of structures, silaffin polypeptides nucleate silicic acid.[97-98] The silica-nucleating silaffin R5 peptide (19 amino acids) from *Cylindrotheca fusiformis* has been produced recombinantly in *E. coli* and used to create engineered silica nanostructures.[99] Natural silaffin polypeptides are highly decorated with post-translational modifications, but it has been shown that the lysines in unmodified R5 peptides bind to the substrate tetramethyl orthosilicate (TMOS) and are sufficient to catalyze silica precipitation.[99-100] We hypothesized that the R5 peptide could form a silica shell around nanoparticles.

R5 contains a charged surface that has been observed to bind to metal surfaces, including titanium.[101] First, we tested commercial metal oxide nanoparticles (Fe_3O_4, TiO_2, Ta_2O_5, and HfO_2) (Figure 4b). Only when the particles were treated with both R5 and TMOS, silica shells were found to form. These reactions were performed for 30 minutes at room temperature (Methods). The shell thickness varied depending on the core material; 22 ± 10, 9 ± 3, 31 ± 11 and 8 ± 3 nm for Fe_3O_4, TiO_2, Ta_2O_5, and HfO_2 particles, respectively. There was no correlation between the shell thickness and electron configuration of the metal core. Purified magnetosomes were then treated with R5 peptide and a silicate shell was observed to form. The concentration of R5 controlled the thickness of the silica, from 3 to 35 nm shells, in a graded manner (Figures 4c,d).

R5 was then fused to MamC (*mamC::R5*) and placed under an IPTG-inducible promoter (Supplementary Figure 37). *M. magneticum* cultures were induced to produce MamC::R5 and the magnetosomes were purified. Magnetosomes expressing MamC::R5 precipitated silica to form a 10 nm shell in the absence of exogenous R5, which is equivalent to wild-type magnetosomes when 300 µM of external R5 is added (Figure 4c,d). However, when the R5 concentration was increased in the reaction with MamC::R5 magnetosomes, the shell thickness was stable at 10 nm until a threshold is reached at 600 µM, after which large silica-only particles predominate.

Discussion

This work presents tools to simplify the genetic engineering of *M. magneticum*. Sweeping through gene expression levels allows the rapid determination of whether IONP properties can be tuned, as opposed to more dramatic impact of a gene knockout. We find that the IONPs produced by the MAI are robust to the overexpression of individual genes. Most have no impact and those that do tend

to produce fewer of the same crystals or immature crystals, as opposed to altering crystal form. The only gene we found that could tune the properties of the crystal itself over a wide range of expression levels, without producing obviously immature crystals, is *mamC*. It may be that more simultaneous changes are required to make different crystal form. This is consistent with the observations that similar species make the same crystal form and size and random mutagenesis changes the number of crystals per cell, but not their shape.[21, 102] In addition, expression timing and checkpoint control during biogenesis has also been seen to be important[70, 94] and magnetosome membrane proteins that control crystal nucleation and growth have interdependent and redundant functions.[30, 45, 51, 103] Therefore, using one chasses to build different IONPs may require the mining of whole operons or MAIs, the balancing of multiple genes, control over membrane invagination, and temporal circuits for gene expression ordering.

Magnetotactic bacteria offer a potential biological route to the production of metal nanoparticles with properties difficult to obtain through chemical synthesis[13, 21, 30, 37] (see review[1] for the advantages and disadvantages of various synthesis techniques). Cells are natural architects to build composite materials that can be rationally designed by combining pathways from different sources, as we have done to produce silica shells around the metal nanoparticles by incorporating proteins from marine eukaryotic diatoms.[99] Understanding the bio-manufacturing of such materials, and the possible products, is still nascent, where metabolic and cost models have focused on carbon-based products. While slow growing, there has been work with fermentation of magnetotactic bacteria and material properties can be controlled with media, growth conditions, and purification.[104-106] Titers of up to 180 mg/L/day have been reported.[104] Further, the magnetosome crystals can be doped by adding metal salts to the media, such as cobalt, and can be chemically processed after recovery.[27, 107-111] Genetic engineering has been applied to increase the IONP titer by adding a second copy of the MAI or transferring it into a species more conducive to bio-production and random mutagenesis of the genome.[72, 102, 112] *E. coli* and yeast have also emerged as promising and more easily engineered chasses for metal nanoparticle bioproduction, despite not being specialized chasses for this purpose.[113-116] New genetic techniques to manipulate complex, multi-gene IONP biogenesis pathways, simple to culture chasses strains, and new techniques for scale-up, purification and cost models are required to fully realize the potential of engineering biology to produce composite nanomaterials.

Materials and Methods

Strains and Plasmids. *M. magneticum* AMB-1 was used for all studies (obtained as a gift from Professor A. Komeili, University of California – Berkeley). *E. coli* NEB 10-beta (NEB) was used for cloning, and *E. coli* WM3064 (also known as BW29427) (*thrB1004 pro thi rpsL hsdS lacZ*ΔM15 RP4-1360 Δ(*araBAD*)567 Δ*dapA*1341::[*erm pir*], obtained from Professor A. Komeili)[77] was used for plasmid conjugation. WM3064 harbors the RP4 conjugation machinery in the genome, and lacks the *dapA* gene and therefore require 2,6-diaminopimelic acid (DAP) to grow. The pMGT-pUC57 plasmid was obtained from Professor P.R. LeDuc (Carnegie Mellon University) and consists of the pMGT plasmid (synthesized based on Genbank accession no. NC_007706) inserted into the EcoRI/HindIII site of pUC57-Amp vector. This pMGT-pUC57 plasmid was used as a template for PCR to construct the pMGA, pMGB and pMGU plasmids (Supplementary Table 4). The p15A origin of replication sequence used in pMGA and pMGB were derived from pACYC184. The pUC origin of replication sequence in pMGU was derived from pUC57. The antibiotic resistance marker sequences were derived from the following plasmids: kanamycin resistance marker (originally from transposon Tn5) was amplified from pBBR1MCS-Kan;[117] ampicillin resistance marker (originally from transposon Tn3) were amplified from pUC57; gentamicin resistance marker (originally from transposon Tn1696) were derived from pMQ75;[118] chloramphenicol resistance marker (from transposon Tn9) were derived from pACYC184; tetracycline resistance marker tetA were derived from pSC101. The RP4 origin of transfer sequence was derived from pRK415. The plasmid backbones and inducible systems described in this work have been deposited in Addgene (#139931-139936). pMGA-Ptac-mamGFDC and pMGA-Ptac-mms6F were constructed by PCR amplifying the *mamGFDC* or *mms6F* cluster region on *M. magneticum* genome and placing downstream a Ptac promoter on pMGA vector (Supplementary Table 1, 2 and Supplementary Figure 35). pMGA-Ptac-mamA, pMGA-Ptac-mamB, pMGA-Ptac-mamC, pMGA-Ptac-mamD, pMGA-Ptac-mamF, pMGA-Ptac-mamG, pMGA-Ptac-mamI, pMGA-Ptac-mamK, pMGA-Ptac-mamL, pMGA-Ptac-mamQ, pMGA-Ptac-mamR, pMGA-Ptac-mamS, pMGA-Ptac-mamT, pMGA-Ptac-mamV, pMGA-Ptac-mms6 and pMGA-Ptac-mmsF were constructed by PCR-amplifying each magnetosome genes (sequence provided in Supplementary Table 1) and placing under the control of a Ptac promoter on pMGA vector (Supplementary Figure 35). The RBS for each gene were computationally designed to reach a translation initiation rate (TIR) of 5000 (Supplementary Table 1). For *mms6* and *mamT* gene, the GTG start codon in the original sequence was replaced with ATG. Annotations of the open reading frame for *mamQ* gene were corrected based on the protein alignment with *M. gryphiswaldense*.[42]

Media and Reagents. Modified *Magnetospirillum* Growth Media (mMSGM) was prepared based on previously-reported Magnetospirillum Growth Media (MSGM)[74, 77] with modifications in the chemical concentration and the autoclave timing. First, a "base" media (mMSGM-base) is prepared by adding the following to 1 L of Milli-Q filtered water: 0.68 g KH_2PO_4 (Fischer Scientific, Pittsburgh, PA, #P380), 0.34 g $NaNO_3$ (Fischer Scientific #S343), 0.37 g tartaric acid (Alfa-Aesar #A13668), 0.37 g succinic acid (Sigma-Aldrich, St. Louis, MO, USA, #398055), 0.05 g sodium acetate (Sigma-Aldrich #S2889), and 0.55 g sodium hydroxide pellet (Macron Fine Chemicals, Avantor, #7708-10). The pH was adjusted to 6.8 by 10 N NaOH, and autoclaved at 121°C for 40 min. The mMSGM-base media could also be prepared as 10× concentration; to do so, the ingredients were added at 10x the above amounts and the pH was adjusted to 6.8 and the mix autoclaved. To prepare 1x mMSGM-base media, 100 mL of the 10x mMSGM-base was mixed with separately autoclaved 900 mL Milli-Q water. In practice, we found that either of these pre-mixes could be stored for up to 2 months. Just before each bacterial culture, the following solutions were added to mMSGM-base to make mMSGM (per 5 mL media): 125 µL of ATCC Trace Mineral Solution (ATCC MD-TMS), 5 µL ATCC Vitamin Supplement (ATCC MD-VS) and 50 µL of 10 mM ferric quinate solution. For the seed culture starting from colony or glycerol stock, mMSGM were used. For the passage culture, 5 µL of 20 mg/mL ascorbic acid solution was added to 5 mL mMSGM, which we call mMSGM-A. The 20 mg/mL ascorbic acid solution were prepared fresh every time by adding 0.1 g of D-ascorbic acid (Sigma #A7506) to 5 mL of Milli-Q filtered water followed by filter-sterilization by passing through a 0.2 µm syringe filter (Pall #4612). Antibiotics in liquid culture were (final concentration): 5 µg/mL kanamycin (GoldBio #K-120-25) or 5 µg/mL gentamicin (GoldBio #G-400-25). Inducer used were isopropyl β-d-1-thiogalactopyranoside (IPTG) (GoldBio #I2481) and anhydrotetracycline (aTc) (Sigma-Aldrich #37919), and 3-oxohexanoyl-homoserine lactone (OC6) (Sigma-Aldrich #K3007). Ferric quinate stock solution (10 mM) was prepared by adding 0.27 g of $FeCl_3$ $6H_2O$ (Sigma-Aldrich #F2877) and 0.19 g of D-(-)-quinic acid (Sigma-Aldrich #138622) to 100 mL Milli-Q filtered water. The crystals of $FeCl_3$ $6H_2O$ need to be broken using a hammer to make it into a powder. The solution was mixed using a magnetic stirrer at room temperature until the powder dissolves (~5 min). Filter-sterilized using Vacuum Filter System (Corning #430756) and keep at room temperature in dark. This solution was used within 4 weeks. mMSGM agar plates (0.8% agar) were prepared as follows: 8 g of Bacto Agar (BD, Franklin Lakes, NJ, USA, #214010) was added to 900 mL Milli-Q filtered water and autoclaved at 121°C for 40 min. After the media was cooled below 60°C, 100 mL of 10× mMSGM-base, 5 mL ATCC

Trace Mineral solution, 1 mL ATCC Vitamin solution and appropriate antibiotics were added and poured to a plastic dish. Antibiotics used in agar plates were 10 µg/mL kanamycin or 10 µg/mL gentamcin as needed. For *E. coli* growth, LB-Miller media (BD, Franklin Lakes, NJ, USA) was used. Antibiotics for *E. coli* were used in the following final concentration: 50 µg/mL kanamycin, 30 µg/mL gentamicin, 100 µg/mL ampicillin, 10 µg/mL tetracyclin, or 33 µg/mL chloramphenicol, as needed. A solution of 100× DAP was made by adding 0.285 g of DAP (Sigma-Aldrich #33240) to 100 mL Milli-Q filtered water while heating on a hot-plate magnetic stirrer, followed by filter-sterilization with 0.2 µm syringe filter (Pall #4612). Phosphate-buffered saline (PBS) were prepared by diluting the 10x PBS solution (Sigma-Aldrich #11666789001) by Milli-Q filtered water.

M. magneticum storage and passaging. Cells were stored as 12.5% glycerol stocks in a -80°C freezer. This was performed by spinning down the 5-25 mL "Second passage" culture (see below) at 4500*g* for 15 min, resuspending the pellet in 750 µL mMSGM media, mixed with filter-sterilized 250 µL 50% glycerol followed by vortex (Vortex-Genie 2, Scientific Industries, Inc. #SI-0236), and immediately storing the aliquot at -80^{o}C. Unless otherwise noted, *M. magneticum* cultures were started by streaking glycerol stocks on mMSGM agar. After streaking the cells, the plates were inserted into a BD GasPak EZ CampyPouch system (BD #260685) or in a Vacu-Quik Jar (Almore International #15000) with 95% N_2 and 5% air and incubated at 30°C for 5 - 7 days until colonies were observed. Tiny colonies (<1 mm diameter) are visible after 4 - 5 days and growing them for an additional 2 - 3 days will result in colonies with approximately 2 mm diameter. The colonies were picked in open air. After experiments, the plates were kept in Vacu-Quik Jar filled with N_2 air (or a plastic bag flushed with nitrogen) and kept at room temperature and used within 2 days.

5 mL culture conditions. Liquid mMSGM media was warmed to 30°C in a water bath. Single colonies were inoculated into the 5 mL of media, and a 10 mL glass vial (Apex Scientific #LAP.18091306) was sealed with a PTFE-silicone septa screw cap (Apex Scientific, #LAP.18031309). The headspace was replaced with N_2 using a vacuum manifold by vacuuming the headspace and adding N_2 gas. This air exchange was repeated three times for each sample. After the gas pressure was released using a needle, 250 µL (5%) of air (which results in approx. 1% final O_2) was injected into each vial using a needle and a syringe. The vial was placed into a water bath at 30°C with

shaking at 60 rpm in an Innova 3100 Digital Water Bath Shaker (Eppendorf, Hamburg, Germany). This seed culture was incubated for 3 days. The 100 µL of seed culture (1:50 dilution) was added to 5 mL of fresh mMSGM-A media, the vial was sealed and air was replaced as described above. The vial was placed in 30°C water bath and shaken at 60 rpm. The cells were subjected to analysis after 48 h (Figures 1, 3, 4a).

2 L culture conditions. The seed culture starting from colony were performed in 5-mL media as described in the above section and incubated for 3 days. For the second-passage culture, 100 mL of mMSGM-A media was prepared in a 130 mL serum bottle (DWK Life Sciences #223748), and 1 mL (1:50) of the seed culture were inoculated. The bottle was sealed with a rubber cap (chemglass life sciences #CG-3022-06), the headspace was replaced with N_2, and 3.5 mL of air was added using a needle and a syringe. The bottle was incubated at 30°C without shaking. For large-scale third-passage culture, mMSGM-A media was prepared in a 1 L or 2 L glass bottles (Corning #13951L, #13952L), 1:50 dilution of second-passage culture were added, and the bottle was filled to the top by adding mMSGM media and the cap was tightened with minimal headspace and incubated at 30°C for 3 days.

Optimization of culture conditions. Figure 1 and Supplemental Figures 1 and 2 show data regarding the optimization of different aspects of the media and growth conditions. This section describes how these experiments were performed. Colony formation on agar plates (Figure 1b). Two types of mMSGM agar plates, either autoclaving the agar together or separately with the mMSGM media, were prepared. *M. magneticum* were cultured starting from a single colony for three days. OD_{565} were measured, and an aliquot (50-100 µL) of cells were plated on agar plates with several dilutions (10^{-1}, 10^{-3}, 10^{-5}). The agar plates were incubated for 7 days until the colonies were visible. Passaging *M. magneticum* culture over 20 days (Figure 1c). Single colonies were inoculated into 5 mL of mMSGM media (described in "5 mL culture conditions" above) and incubated for 2.5 days. The 100 µL of seed culture (1:50 dilution) was added to 5 mL of fresh mMSGM-A media, air was replaced as described above, and placed in 30°C water bath and shaken at 60 rpm. After the cells were incubated for 2 days, OD_{565} and C_{mag} were measured by using 1 mL of culture ("Cell density (OD_{565}) and magnetic response (C_{mag}) measurement", described below). Inoculation of aliquot (100 µL) to

fresh 5 mL mMSGM-A media, 2-day incubation at 30°C, and OD_{565} and C_{mag} measurement was repeated up to 20 days. The experiment were performed in duplicates starting from 2 independent colonies. Optimization of *M. magneticum* culture (Figure 1d). The unoptimized culture (left panel in Figure 1d) were performed as follows. The media ("unoptimized-mMSGM") was prepared with slight modification to the mMSGM media: 0.12 g of $NaNO_3$ was added to 1-L media (final $NaNO_3$ concentration of 1.4 mM), and 35 mg ascorbic acid to 1-L media was added prior to autoclave. A single colony was inoculated in unoptimized-mMSGM media, the vial was sealed and air was replaced as described in "5 mL culture conditions" in Methods, and incubated for 3 days at 30°C at 60 rpm. This seed culture were inoculated into a 5 mL unoptimized-mMSGM media, the vial was sealed and air replaced as described above, and incubated at 30°C at 60 rpm. After 2 days, the cells were subjected to TEM analysis. The optimized culture (right panel in Figure 1d) were performed as described in "5 mL culture conditions" in Methods described above. Impact on the growth and magnetic response of cells when ascorbic acid was added before or after autoclave (Supplementary Figure 1a). The media with ascorbic acid added before autoclave was prepared as follows. To 500 mL water, the chemicals for mMSGM-base media and D-ascorbic acid (Sigma-aldrich #A7506) (final concentration of 30, 10, 3, 1, 0.3, 0.1, or 0.03 mg/L) were added. The media was autoclaved at 121°C for 40 min and used within 1 week. The media with ascorbic acid added after autoclave is mMSGM-A. These two kinds of media (ascorbic acid added before or after autoclave) were aliquoted (5 mL each) in a 10 mL glass vial. A large piece (approx. 3 mm diameter) of frozen glycerol stocks of wild-type *M. magneticum* cells were directly inoculated in the media. The vial was sealed with a PTFE-silicone septa screw cap, headspace replaced by 95% N2 and 5% air, and placed into a water bath at 30°C at 60 rpm. After 2 days, 1-mL culture were collected, and OD_{565} and C_{mag} were measured. Optimization of reducing agents (Supplementary Figure 1b). Wild-type *M. magneticum* cells from glycerol stocks were inoculated in mMSGM media and cultured for three days. A 100 µL aliquot of this pre-culture was transferred into a 10 mL glass vial containing 5 mL mMSGM media supplemented with different concentrations of reducing agents: ascorbic acid (Sigma-aldrich #A7506), sodium thioglycolate (Sigma-Aldrich #T0632), sodium thiosulfate (Sigma-Aldrich #72049) with final concentration in 500, 100, 20, 4, and 0.8 mg/L. The stock solution for the chemicals were prepared each time just before inoculation by adding 0.1 g of each powder to 5 mL of Milli-Q water followed by filter-sterilization (0.2 µm syringe filter, Pall #4612). The vial was sealed with a PTFE-silicone septa screw cap, headspace replaced by 95% N2 and 5% air, and placed into a water bath at 30°C at 60 rpm. After 2 days, 1 mL culture were collected, and OD_{565} and C_{mag} were measured.

Optimization of inoculation cell amount, ascorbic acid and oxygen concentration (Supplementary Figure 1c). Wild-type *M. magneticum* cells from glycerol stocks were inoculated in mMSGM media and cultured for three days. To determine the cell number per 1 unit of OD_{565}, the pre-culture was plated on an mMSGM agar and incubated for 1 week and the colonies were counted (this yielded OD_{565} 1.0 = 5 x 10^8 cells). Aliquots (100 µL or 1 µL) of pre-culture were inoculated to a 5-mL mMSGM media (resulting in initial OD_{565} of 0.001 or 0.00001, respectively). The media was supplemented with different concentration of ascorbic acid (500, 100, 20, 4, 0.8 or 0 µM) in a 10 mL glass vial and the vials were sealed with a PTFE-silicone septa screw cap. To provide the final concentration of 1%, 5% and 10% O_2 in the headspace, the gas was first replaced with 100% N_2 using a vacuum manifold. The pressure of the headspace was released by a needle and then 50, 250 or 500 µL volume of the gas were sucked out using a syringe and a needle and the same volume of 100% O_2 was injected, resulting in the final concentration of 1%, 5% or 10% O_2 in the headspace. To prepare samples with 20% O_2, the headspace gas was left as it is (filled with air) after the vial was sealed. These vials were placed into a water bath (Innova 3100 Digital Water Bath Shaker) at 30°C and shaken at 60 rpm. After 2 days, 1 mL of culture were collected, and OD_{565} and C_{mag} were measured. Optimization of shaking speed (Supplementary Figure 1d). The experiment was performed as described in "Optimization of inoculation cell amount, ascorbic acid and oxygen concentration" (100 µL pre-culture inoculation), except for the difference in the shaking speed and the incubator shaker. For these experiments at 0, 60 and 120 rpm, the water bath (Innova 3100 Digital Water Bath Shaker) were used; for 240 rpm, New Brunswick Innova 44 shaker (Eppendorf) was used. Optimization of sodium nitrate concentration (Supplementary Figure 2). mMSGM-A media containing sodium nitrate concentration of 0, 0.4, 1.4, 4 and 10 mM were prepared by adding a filter-sterilized 2 M sodium nitrate solution ($NaNO_3$, Fischer Scientific #S343) to a $NaNO_3$-lacking mMSGM-A media. Wild-type *M. magneticum* cells from glycerol stocks were inoculated in mMSGM media and cultured for three days. A 100 µL aliquot of cells were transferred to 5 mL mMSGM-A media with various nitrate concentrations in 10 mL glass vial, and the vials were sealed with a PTFE-silicone septa screw cap. The headspace was replaced with 95% N_2 + 5% air, and cultured at 30°C, 60 rpm in a water bath (Innova 3100 Digital Water Bath Shaker). The cells were collected after 2 days and analyzed by TEM.

Transformation of M. magneticum. Plasmid conjugation was used to transfer plasmid DNA from *E. col* into *M. magneticum*. The plasmids were electroporated into *E. coli* WM3064 and plated on LB

agar supplemented with 150 µM DAP with appropriate antibiotics. The *E. coli* colonies were inoculated with 3 mL LB media supplemented with 150 µM DAP and cultured overnight (12-15 hours). *M. magneticum* cultures were obtained from the pre-culture (after 3 days) or second passage (after 2 days, OD_{565} of 0.3 to 0.5) described above. One mL of *M. magneticum* culture and 100 µL of *E. coli* overnight culture were mixed in a 1.5 mL microcentrifuge tube (Fischer # 05-408-129) and centrifuged at 10,000*g* for 1 min using an Eppendorf Centrifuge 5481. The cell pellet was resuspended with 1 mL mMSGM media, followed by centrifugation for 1 min. After discarding the supernatant with pipette, the cells were resuspended in the residual media (approximately 5 µL), and this was spotted on a mMSGM agar plate supplemented with 15 µM DAP (the agar plate were pre-dried in a fume hood for ~30 min so that the spotted liquid will dry faster). The plates were placed in a ziploc bag, and N_2 gas were added to the bag until fully inflated, and incubated at 30°C for 6-8 hours. The spotted cells were collected using an inoculation loop and resuspended into 100 µL mMSGM media. Several dilutions of the cells were plated on a mMSGM agar supplemented with antibiotics, placed in Vacu-Jar or BD CampyPouch, and incubated at 30°C for 5-7 days to obtain colonies.

Magnetosome purification. The protocol to purify magnetosomes was designed based on published methods[80, 96] with some modifications. HEPES buffer (20 mM, pH 7.3) were prepared by adding 20 mL of 1 M HEPES Solution pH 7.3 (Affymetrix, Inc. Cleveland, OH, #16924) to 980 mL of Milli-Q filtered water. HEPES-E buffer used for magnetosome purification was prepared by adding 500 µL of 1 mM EDTA (USB Corporation, Cleveland, OH, #15694) to 1 L of the 20 mM HEPES (pH 7.3) buffer. The *M. magneticum* culture (1.2 L) was divided into 600 mL volumes into 1 L centrifuge bottles (Thermo Scientific, Nalgene PPCO bottles 05-562-25) and centrifuged at 5000*g* for 20 min (Thermo scientific Sorval RC 6+ centrifuge & fiberlite F10-4x1000 LEX roter). The cell pellet was resuspended with 50 mL of HEPES-E, transferred to 250 mL centrifuge bottles (Thermo Scientific, Nalgene PPCO bottles 3141-0250) and centrifuged at 5000*g* for 20 min (Thermo scientific fiberlite F14-6x250y roter). The cell pellet was kept at 4°C if not immediately used. The cell pellet was "softened" by vortexing the bottle at the maximum setting (Vortex-Genie 2, Scientific Industries, Inc. #SI-0236). The cells were resuspended in HEPES-E until the cell clump was not visible. The cells were passed through a French Press (Constant Systems Ltd. CF Cell Disrupter, Dr. Tania Baker lab at MIT) at 20 kpsi. The lysate was transferred to a 250 mL centrifuge bottle and was sonicated on ice for 1

min at 10% amplitude with 1-sec ON/OFF interval (Sonic Dismembrator 500, Fisher Scientific, Waltham, MA, USA). The lysate were transferred to a 50-mL falcon tube (Corning #352070) and placed next to a Neodymium-Iron-Boron (NdFeB) magnet (Permagen #MSR6x50) and left overnight at 4°C. After discarding the supernatant, the magnetic fraction was resuspended into 10 mL HEPES-E, sonicated for 30 sec (10% amplitude, 1-sec ON/OFF interval), and placed next to a NdFeB magnet for over 2 hours. The collected magnetic fraction was resuspended in 2 mL Milli-Q water. When removing the membrane, the magnetic fraction was resuspended in 2 mL 1% sodium dodecyl sulfate (Sigma-Aldrich #436143) solution and incubated for 16 hours with gentle shaking (Nutator, VWR, Ranor, PA, USA). The magnetosomes were collected by NdFeB magnet for 1 hour, resuspended in Milli-Q filtered water and sonicated for 10 sec (10% amplitude, 1-sec ON/OFF innterval) and resuspended in 2-mL Milli-Q filtered water.

Transmission Electron Microscopy (TEM). A 5 µL aliquot of the *M. magneticum* culture was placed onto a carbon/formvar-coated TEM copper grid (Electron Microscopy Sciences #FCF200-Cu). After waiting for 30 sec to 5 min for the *M. magneticum* cells to land on the copper grid surface, the liquid was removed by absorbing with a kimwipe (Kimberly-Clark #34120). When absorbing the liquid, we left a small amount of liquid (less than 1 µL) on the surface to avoid removing the cells. The copper grid was dried briefly (approximately 5 min) in the fume hood until the remaining liquid was dried completely. To wash the salts/impurities, 5 µL of Milli-Q filtered water were placed on the grid, absorbed with a kimwipe, and the grid was dried in fume hood for 10 mins. The purified magnetosomes in Milli-Q filtered water was dispersed by tip sonication for 1 sec at 10% amplitude on ice. Five µL of the sonicated magnetosome solution were placed on a carbon/formvar-coated TEM copper grid, and after 30 sec to 5 min, the liquid were removed by a kimwipe, and dried in the fume hood for 5 min. The grid surface was washed by adding 5 µL of Milli-Q filtered water followed by removing the liquid by a kimwipe and the grid was dried in the fume hood for 10 min. The TEM grid samples were analyzed using a Tecnai G2 Spirit TWIN (Hillsboro, OR, USA) operating at 120 kV (Electron Microscopy lab at the Center for Materials Science and Engineering CMSE, MIT), and images were collected at 6500× and 26000× magnification. TEM images at 26000× magnification were used for image analysis using Fiji/ImageJ. The noise in the image was smoothed by applying a mean filter (1.5 pixels). The scale bar was removed from the image and the particles were masked by autothresholding using the "Triangle" method. The “Analyze particle” command was used to

calculate the minimum/maximum Feret diameter and the major/minor axis of the fitted ellipse. The data used to create the histograms in Figure 3 were chosen by randomly sampling 150 particles from the Fiji/ImageJ TEM image analysis results. Random sampling of the particles was implemented using the built-in function sample() of the DataFrame class in the python pandas library. The diameter/shape-factor plot was drawn by randomly sampling 500 particles from the Fiji/ImageJ image analysis results of the purified magnetosomes. The shape factor (described in main text) and the diameter (major axis of the fitted ellipse) were plotted. The magnetosome particle images in Figure 3 were drawn by randomly sampling 20 particles by using sample() method of the pandas DataFrame class in python. Each particle image was cropped into a rectangular shape from the original TEM image and pasted in to a new canvas to create a temporary image. The TEM background (grey-colored region surrounding each particles) in this image were removed as follows. The "Analyze particle" command in Fiji/ImageJ was applied to the temporary image and created a "mask" that only selects for a round-shaped particle. Using Photoshop, the masked region was inverted and used to delete the non-particle background. The selected particles are shown in the context of the greater images as boxes in Supplementary Figures 28-30. The frequency of longest magnetosome chain per cell (Figure 3m) were calculated as follows. For each cells observed in the TEM image, the longest magnetosome chain without gaps were identified, and the numbers of magnetosome particles were counted. The histograms were drawn using the bin width of 5. The frequency were normalized by dividing the values with the number of total cells analyzed (48 and 32 for mamK and wild-type cells, respectively). To make the histogram in Supplementary Figure 27d, the numbers of magnetosome particles in one cells were counted and histograms were generated using the bin width of 5. The frequency were normalized by the number of cells (48 and 32 for mamK and wild-type cells, respectively).

Cell density (OD_{565}) and magnetic response (C_{mag}) measurement. M. magneticum cell growth was monitored by measuring OD at 565 nm (OD_{565}). The 565 nm wavelength was chosen by following the previous reports.[73, 119] Undiluted cells were placed in a plastic 1 cm cuvette and the OD_{565} was measured using Agilent Cary 60 UV-Vis Spectrometer. The magnetosome production of the cells was monitored using a light-scattering assay[77, 120] to measure the "magnetic response" (C_{mag}) with slight modification. A bar magnet (VWR #58947-128) was placed parallel or perpendicular to the cuvette holder of Agilent Cary 60 UV-Vis Spectrometer, and the maximum and minimum absorbance (OD_{max}

and OD_{min}) at 565 nm were recorded. C_{mag} was calculated by OD_{max} / OD_{min}.

Flow cytometry analysis. Fluorescence was measured using a MACSQuant® VYB Analyzer (Miltenyi Biotec, Germany) with a 488-nm laser for GFP excitation. The FlowJo v10 (TreeStar Inc.) software was used to analyze the data. All events were gated by forward scatter and side scatter and at least 30,000 events were collected for each sample. The geometric mean of each sample was calculated.

Plasmid stability measurements. Single colonies were inoculated into 5 mL mMSGM media with kanamycin in a 10 mL glass vial and sealed with a PTFE-silicone septa screw cap. The headspace was replaced with N_2 by vacuuming the headspace and adding N_2 gas and repeating this process three times. After the gas pressure was released using a needle, 250 µL (5%) of air was injected into each vial using a needle and a syringe. The vial was cultured in a water bath (Innova 3100 Digital Water Bath Shaker) at 30°C at 60 rpm. After 3 days, 78 µL of the culture was inoculated into fresh 5 mL mMSGM-A (1:64 dilution) without antibiotics and cultured for 48 hours (8 generations). The passage into mMSGM-A media with 1:64 dilution was repeated 4 times to reach 32 generations. From each passage, 10 µL of culture was collected from each passage (just before inoculation) and added to 200 µL of chilled PBS with 2 mg/mL kanamycin in a 96-well plate. The plate was kept at 4°C for >24 hours, and then analyzed using flow cytometry.

Promoter mining. The upstream sequence region of the 16S rRNA gene in the *M. magneticum* genome (NC_007626.1, nucleotides 964,286 to 964,756) were used to search for the promoters using Berkeley Drosophila Genome Project promoter prediction software (with minimum promoter score of 0.8) (https://www.fruitfly.org/seq_tools/promoter.html) (Supplementary Figure 7). Four promoters were predicted, and we defined the promoter sequence as the transcription start site and 35 bases upstream as P_{rrn1}, P_{rrn2}, P_{rrn3} and P_{rrn4} (P_{rrn1} and P_{rrn2} had an exact same sequence). Constitutive promoters parts are derived from the Registry of Standard Biological Parts[85] (BBa_J23101, BBa_J23104, BBa_J23111, BBa_J23117, BBa_J23119), and the exact sequence were used. P_{neokan} promoter is derived from the Tn5 kanamycin resistance marker cassette. $P_{mamDC45}$ is derived from ref. [61]. P_{mms16}, P_{msp1} and P_{msp3} were identified from the literature.[63]

Promoter strength measurements. *M. magneticum* cells harboring plasmids were streaked from glycerol stocks to a mMSGM agar plate. Colonies were picked into 5 mL mMSGM media supplemented with kanamycin in a 10- mL glass vial, sealed with a PTFE-silicone septa screw cap. The headspace was replaced with N_2 by vacuuming the headspace and adding N_2 gas and repeating this process three times. After the gas pressure was placed using a needle, 250 µL (5%) of air was injected into each vial using a needle and a syringe. The vial was cultured in a water bath at 30°C at 60 rpm for 3 days. A 100 µL aliquot of this pre-culture were passaged to 5 mL mMSGM-A supplemented with kanamycin. The head space was replaced with N_2, repeated three times, and 5% air were injected. The vial was cultured at 30°C at 60 rpm. After 48 hours, 10 µL of culture was combined with 200 µL of chilled PBS supplemented with 2 mg/mL kanamycin in a 96-well plate. The plate was kept at 4°C refrigerator for 24 hours and then analyzed using flow cytometry. For promoter measurements in *E. coli*, the plasmids were transformed into *E. coli* NEB 10-beta. Individual colonies were picked into 600 µL LB media supplemented with kanamycin in a 96-well deep-well plate (USA Scientific, Orlando, FL, USA) sealed with AeraSeal film (Excel Scientific, Victorville, CA, USA) and grown at 37°C and 900 rpm overnight in a Multitron Pro shaker incubator (INFORS HT, Bottmingen, Switzerland). An aliquot of 1 µL was then transferred to fresh 500 µL with Kan in a 96-well deep-well plate and cultured at 37°C at 900 rpm for 6 hours. Then, a 5 µL aliquot is transferred to chilled PBS supplemented with 2 mg/mL kanamycin in a 96-well plate and kept at 4°C for 24 hours and analyzed using flow cytometry.

Computational RBS design. The RBS Library Calculator v2.0[86-88] (www.denovodna.com) was used. The 16S rRNA was set as *Magnetospirillum magneticum* AMB-1 (ACCTCCTTT); pre-sequence (TCTAGAAATAATTTTGTTTATCTCTC); first 50 bp of coding sequence (ATGCGTAAAGGCGAAGAGCTGTT-CACTGGTGTCGTCCCTATTCTGGTGGA); targeted maximum TIR 100,000; targeted minimum TIR 1, target library size 36. Among the 10 obtained library candidates, we selected the sequence AAAGTCACCGAGAWCAAGATAAASGSGSTARAAC (degenerate codon underlined), a 32-variant library with maximum TIR of 28,086 and minimum TIR of 2 with 64% coverage, which had the sequence. We chose 14 of these RBSs (Table 1 R01 to R14; TIR 2 to 28086). To test additional RBSs higher than 28,086, we also chose two RBS sequences from another library (Table 1, R15 and R16; TIR 46078 and 66844). These RBS sequences (16 total) were synthesized and

cloned into a plasmid under two different promoters, BBa_J23119 and BBa_J23117.

RBS measurements. The 16 plasmids with different RBSs under the control of the BBa_J23119 promoter were pooled together. The pooled plasmids were conjugated into *M. magneticum* and spread on agar plates to obtain >50 colonies. Colony PCR of the RBS region was performed for 32 colonies and the sequences verified. The same procedure was performed for BBa_J23117- based RBS variants. The colonies corresponding to sequenced RBSs were inoculated into 5 mL mMSGM media supplemented with kanamycin in a 10 mL glass vial and sealed with a PTFE-silicone septa screw cap. The headspace was replaced with N_2 by vacuuming the headspace and adding N_2 gas and the process repeated three times. After the gas pressure was released using a needle, 250 µL (5%) of air was injected into each vial using a needle and a syringe. The vial was cultured in a water bath at 30°C at 60 rpm for 3 days. A 100 µL aliquot of this pre-culture were passaged to 5 mL mMSGM-A supplemented with kanamycin. The head space was replaced with N_2, repeated three times, and 5% air were injected. The vial was cultured at 30°C at 60 rpm. After 48 hours, 10 µL of culture was combined with 200 µL of chilled PBS supplemented with 2 mg/mL kanamycin in a 96-well plate. The plate was kept at 4°C refrigerator for 24 hours and then analyzed using flow cytometry.

Measurement of inducible system response. The *M. magneticum* cells harboring plasmids were streaked from glycerol stocks to a mMSGM agar plate. Colonies were picked into 5 mL mMSGM media supplemented with kanamycin in a 10 mL glass vial and sealed with a PTFE-silicone septa screw cap. The headspace was replaced with N_2 by vacuuming the headspace and adding N_2 gas and the process repeated three times. After the gas pressure was released using a needle, 250 µL (5%) of air was injected into each vial using a needle and a syringe. The vial was cultured in a water bath at 30°C at 60 rpm for 3 days. A 100 µL aliquot of this pre-culture were passaged to 5 mL mMSGM-A supplemented with kanamycin and inducers. The head space was replaced with N_2, repeated three times, and 5% air were injected. The vial was cultured at 30°C at 60 rpm. After 48 hours, 10 µL of culture was combined with 200 µL of chilled PBS supplemented with 2 mg/mL kanamycin in a 96-well plate. The plate was kept at 4°C refrigerator for 24 hours and then analyzed using flow cytometry.

Induction experiments for expressing MAI genes, mamC::R5 and mamC::sfgfp. The *M. magneticum* cells harboring plasmids were streaked from glycerol stocks to a mMSGM agar plate. Colonies were picked into 5 mL mMSGM media supplemented with kanamycin in a 10 mL glass vial, sealed with a PTFE-silicone septa screw cap. The headspace was replaced with N_2 by vacuuming the headspace and adding N_2 gas and the process repeated three times. After the gas pressure was released using a needle, 250 µL (5%) of air was injected into each vial using a needle and a syringe. The vial was cultured in a water bath at 30°C at 60 rpm for 3 days. A 100 µL aliquot of this pre-culture were passaged to 5 mL mMSGM-A media supplemented with kanamycin and inducers. The head space was replaced with N_2, repeated three times, and 5% air were injected. The vial was cultured at 30°C at 60 rpm. After 48 hours, the cells were subjected to TEM analysis.

Fluorescent microscope analysis. The fluorescence microscope in Figure 1i and 4a were performed as follows. Agarose pads were prepared by flanking a 200 µL of microwaved 1% agarose solution by two coverslips and solidifying at room temperature for 30 min. The agar pad was placed on a microscope slide, and the sample (cell culture or purified magnetosome solution) were placed on the agar pad and covered with a cover slip. The microscope image was captured on a Zeiss Axiovert 200M microscope equipped with 1,344 × 1,024 pixel cooled ORCA-ER CCD camera (Hamamatsu Corporation) and a × 100 objective. The filter used were 500/20 (excitation) and 535/50 (emission). The Data collection and processing were performed using AxioVision software (Zeiss).

Preparation and analysis of silica-coated particles. Purified R5 peptide was produced from recombinant *E. coli*, following the protocol described previously [99]. Lyophilized peptide was reconstituted at 5 mM in autoclaved Milli-Q water. Silica reactions were performed in 44 µL liquid volumes in 1.5 mL microcentrifuge tubes (USA Scientific #1415-2500). 36 µL of R5 peptide concentrations (0 – 500 µM) were prepared in 30 mM NaH_2PO_4 (USB #20233). Metal oxide nanoparticle powders of Fe_3O_4 (Sigma #900081, 30 nm average dia.), TiO_2 (Sigma #637254, < 24 nm dia.), HfO_2 (Sigma #202118), Ta_2O_5 (Sigma #303518), ZnO (Sigma #677450, < 50 nm dia.) were prepared in 30 mM NaH_2PO_4, pH 7.5 at 1 mg/mL concentration. Wild-type magnetosomes were purified as described above and then incubated in 20 mM CAPS at pH 11.0 for 16 hours with gentle

shaking (Nutator, VWR, Ranor, PA, USA) at 4˚C. Magnetosomes were sonicated (10% amplitude, 1 second pulse + 1 second pause, 1 minute sonication) (Sonic Dismembrator 500, Fisher Scientific, Waltham, MA, USA) and then collected by a magnet over 1 hour at 4˚C. Collected magnetosomes were washed in 20 mM HEPES-E (20 mM HEPES, pH 7.4, 0.5 mM EDTA), sonicated (10% amplitude, 1 second pulse + 1 second pause, 30 seconds sonication), and collected again by a magnet for 1 hour at 4˚C. Collected magnetosomes were resuspended in 5 mL HEPES-E and purified by ultracentrifugation as described above. Purified magnetosomes were collected by placing a NdFeB magnet next to the microcentrifuge tube for 5 minutes and resuspended to 1 mg/mL in 30 mM NaH_2PO_4 (USB #20233) at pH 7.5. The metal nanoparticles and magnetosomes were sonicated (10% amplitude, 0.5 second pulse + 0.5 second pause, 10 seconds sonication) and 4 µL was immediately pipetted into the R5-phosphate solution. Tubes were briefly vortexed and then incubated without mixing for 1 hour at room temperature. 1 M tetramethyl orthosilicate (TMOS, Sigma #341436) was freshly hydrolyzed in 1 mM HCl for 30 min prior to performing the silica reaction. Silification reactions were initiated with the addition of 4.4 µL hydrolyzed TMOS (100 mM final concentration) to the peptide-nanoparticle solution, briefly vortexed, and then incubated without mixing for 30 minutes at room temperature. After 30 minutes, 10 µL of the reaction mixture was spotted onto TEM grids (EMS #FCF200-CU). After 3 minutes, excess liquid was wicked away using kim-wipe or blotting paper and the nanoparticles were washed three times with 10 µL ddH_2O. The nanoparticles were imaged by TEM. Silica shell thickness was manually analyzed using ImageJ software.

XPS, FTIR and XRD measurements. *M. magneticum* cells (wild-type or strains harboring pMGA-P_{tac}-mms6 or pMGA-P_{rrn34}-mamC) were cultured and magnetosomes were purified with the membrane intact as described in Supplementary Note 1, and were stored in deionized (DI) water. The magnetosome solutions were kept at 4°C overnight so that the particles sediment to the bottom of the tube. An aliquot (5 µL for XPS and FTIR, 10 µL for XRD) of the magnetosome suspension was collected from the bottom of the tubes and placed on copper tape (XPS, FTIR) or silica glass (XRD) and dried for at least one day until the water completely evaporated to make dry films. The copper tape supported samples were mounted onto a PHI VersaProbe III. A monochromatic Al K_α X-ray source was used to collect XPS data to assess surface elemental composition and valence. The FTIR measurements were performed by mounting the copper tape supported samples onto an Alpha FTIR spectrometer (Bruker Optics Inc.: Billerica, MA, USA) with a diamond attenuated total reflection

attachment was used to assess the chemical functional groups present. The XRD measurements were taken by placing the glass-substrate supported samples on a Panalytical X'Pert^3 XRD system with the data collected over a range 10°-90° for 2θ.

Magnetization hysteresis. The magnetosomes were first extracted from the suspension via centrifuge and syringe then mounted onto 8 mm glass fiber filter paper. After 48 hours drying, the filter paper samples were mounted onto the quartz rod sample holder for a MicroSense Vibrating Sample Magnetometer. Magnetization versus applied magnetic field measurements were taken from +/- 6.5 kOe at room temperature, and the magnetization values were then normalized to the apparent saturation magnetization and plotted.

Acknowledgements

This work was supported by the Institute for Collaborative Biotechnologies through cooperative agreement W911NF-19-2-0001 and W911NF-19-2-0026 with the U.S. Army Research Office. C.A.V. thanks the Wright Brothers Institute (WBI) for the Synthetic Biology Challenge Prize. We thank Prof. Arash Komeili (UC Berkeley) for wild-type *M. magneticum* AMB-1 and *E. coli* WM3064. We thank Prof. Ron Weiss (MIT) for the use of fluorescence microscope, Dr. Tania Baker (MIT) for the use of French press, and Dr. Yong Zhang (CMSE, MIT) for assistance with TEM. Synthesized pMGT was built by L.G. and received from Prof. P.R. LeDuc (Carnegie Mellon University).

References

[1] A. Ali, M. Z. Hira Zafar, I. ul Haq, A. R. Phull, J. S. Ali, A. Hussain, *Nanotechnol. Sci. Appl.* **2016**, 9, 49.

[2] E. A. Campos, D. V. B. S. Pinto, J. I. S. d. Oliveira, E. d. C. Mattos, R. d. C. L. Dutra, *J. Aerosp. Technol. Manag.* **2015**, 7, 267.

[3] S. Hasany, N. Abdurahman, A. Sunarti, R. Jose, *Curr. Nanosci.* **2013**, 9, 561.

[4] F. J. Owens, C. P. Poole Jr, *The physics and chemistry of nanosolids*, John Wiley & Sons, **2008**.

[5] C. W. Kartikowati, Q. Li, S. Horie, T. Ogi, T. Iwaki, K. Okuyama, *RSC Advances* **2017**, 7, 40124.

[6] L. H. Reddy, J. L. Arias, J. Nicolas, P. Couvreur, *Chem. Rev.* **2012**, 112, 5818.

[7] M. Zahn, *J. Nanopart. Res.* **2001**, 3, 73.

[8] S. Tong, C. A. Quinto, L. Zhang, P. Mohindra, G. Bao, *ACS nano* **2017**, 11, 6808.

[9] A. K. Gupta, M. Gupta, *Biomaterials* **2005**, 26, 3995.

[10] W. Wu, Z. Wu, T. Yu, C. Jiang, W.-S. Kim, *Sci. Technol. Adv. Mater.* **2015**, 16, 023501.

[11] S. Laurent, S. Dutz, U. O. Häfeli, M. Mahmoudi, *Adv. Colloid Interface Sci.* **2011**, 166, 8.

[12] W. Wang, Q. Li, A. Zheng, X. Li, Z. Pan, J. Jiang, L. Zhang, R. Hong, L. Zhuang, *Results Phys.* **2019**, 14, 102366.

[13] T. Prozorov, D. A. Bazylinski, S. K. Mallapragada, R. Prozorov, *Mater. Sci. Eng. R Rep.* **2013**, 74, 133.

[14] A. S. Teja, P.-Y. Koh, *Prog. Cryst. Growth Charact. Mater.* **2009**, 55, 22.

[15] A. Figuerola, R. Di Corato, L. Manna, T. Pellegrino, *Pharmacol. Res.* **2010**, 62, 126.

[16] C. Li, Y. Shen, M. Jia, S. Sheng, M. O. Adebajo, H. Zhu, *Catal. Commun.* **2008**, 9, 355.

[17] Z. Ma, F. Li, H. Bai, *Propellants Explos. Pyrotech.* **2006**, 31, 447.

[18] F. Shi, M. K. Tse, M. M. Pohl, A. Brückner, S. Zhang, M. Beller, *Angew. Chem. Int. Ed.* **2007**, 46, 8866.

[19] M. Appl, *Ullmann's encyclopedia of industrial Chemistry* **2000**.

[20] D. Koulialias, I. García-Rubio, L. Rahn-Lee, A. Komeili, J. F. Löffler, A. U. Gehring, M. Charilaou, *J. Appl. Phys.* **2016**, 120, 083901.

[21] G. Vargas, J. Cypriano, T. Correa, P. Leao, D. A. Bazylinski, F. Abreu, *Molecules* **2018**, 23.

[22] S. Laurent, D. Forge, M. Port, A. Roch, C. Robic, L. Vander Elst, R. N. Muller, *Chem. Rev.* **2008**, 108, 2064.

[23] K. Hola, Z. Markova, G. Zoppellaro, J. Tucek, R. Zboril, *Biotechnol. Adv.* **2015**, 33, 1162.

[24] H. Choi, J.-P. Lee, S.-J. Ko, J.-W. Jung, H. Park, S. Yoo, O. Park, J.-R. Jeong, S. Park, J. Y. Kim, *Nano Lett.* **2013**, 13, 2204.

[25] H. Zhu, C. Tang, L. Fonseca, R. Ramprasad, *J. Mater. Sci.* **2012**, 47, 7399.

[26] J. Cichos, M. Karbowiak, *J. Mater. Chem. B* **2014**, 2, 556.

[27] S. Borg, D. Rothenstein, J. Bill, D. Schuler, *Small* **2015**, 11, 4209.

[28] S. Spring, D. A. Bazylinski, in *The Prokaryotes: Volume 2: Ecophysiology and Biochemistry* **2006**, p. 842.

[29] D. Schüler, *Magnetoreception and Magnetosomes in Bacteria*, Springer-Verlag Berlin Heidelberg, **2007**.

[30] D. Faivre, *MRS Bull.* **2015**, 40, 509.

[31] T. Prozorov, *Semin. Cell Dev. Biol.* **2015**, 46, 36.

[32] R. Uebe, D. Schuler, *Nat. Rev. Microbiol.* **2016**, 14, 621.

[33] A. Komeili, *FEMS Microbiol. Rev.* **2012**, 36, 232.

[34] M. Pósfai, C. Lefèvre, D. Trubitsyn, D. A. Bazylinski, R. Frankel, *Front. Microbiol.* **2013**, 4, 344.

[35] A. Arakaki, H. Nakazawa, M. Nemoto, T. Mori, T. Matsunaga, *J. R. Soc. Interface* **2008**, 5, 977.

[36] T. Yoshino, Y. Maeda, T. Matsunaga, *Recent Pat. Biotechnol.* **2010**, 4, 214.

[37] F. Mickoleit, D. Schüler, *Bioinspired Biomimetic Nanobiomater*. **2018**, 8, 86.

[38] E. Alphandéry, I. Chebbi, F. Guyot, M. Durand-Dubief, *Int. J. Hyperthermia* **2013**, 29, 801.

[39] S. Ullrich, M. Kube, S. Schubbe, R. Reinhardt, D. Schuler, *J. Bacteriol.* **2005**, 187, 7176.

[40] A. Lohsse, S. Ullrich, E. Katzmann, S. Borg, G. Wanner, M. Richter, B. Voigt, T. Schweder, D. Schuler, *PLOS ONE* **2011**, 6, e25561.

[41] D. Murat, A. Quinlan, H. Vali, A. Komeili, *Proc. Natl. Acad. Sci. U. S. A.* **2010**, 107, 5593.

[42] A. Lohsse, S. Borg, O. Raschdorf, I. Kolinko, E. Tompa, M. Posfai, D. Faivre, J. Baumgartner, D. Schuler, *J. Bacteriol.* **2014**, 196, 2658.

[43] H. C. McCausland, A. Komeili, *PLoS Genet.* **2020**, 16, e1008499.

[44] A. Scheffel, A. Gardes, K. Grunberg, G. Wanner, D. Schuler, *J. Bacteriol.* **2008**, 190, 377.

[45] M. Tanaka, E. Mazuyama, A. Arakaki, T. Matsunaga, *J. Biol. Chem.* **2011**, 286, 6386.

[46] D. Murat, V. Falahati, L. Bertinetti, R. Csencsits, A. Kornig, K. Downing, D. Faivre, A. Komeili, *Mol. Microbiol.* **2012**, 85, 684.

[47] O. Raschdorf, F. Bonn, N. Zeytuni, R. Zarivach, D. Becher, D. Schuler, *J. Proteomics* **2018**, 172, 89.

[48] A. Arakaki, J. Webb, T. Matsunaga, *J. Biol. Chem.* **2003**, 278, 8745.

[49] A. Taoka, R. Asada, H. Sasaki, K. Anzawa, L. F. Wu, Y. Fukumori, *J. Bacteriol.* **2006**, 188, 3805.

[50] H. Nudelman, C. Valverde-Tercedor, S. Kolusheva, T. P. Gonzalez, M. Widdrat, N. Grimberg, H. Levi, O. Nelkenbaum, G. Davidov, D. Faivre, *J. Struct. Biol.* **2016**, 194, 244.

[51] S. S. Staniland, A. E. Rawlings, *Biochem. Soc. Trans.* **2016**, 44, 883.

[52] A. Yamagishi, K. Narumiya, M. Tanaka, T. Matsunaga, A. Arakaki, *Sci. Rep.* **2016**, 6, 35670.

[53] H. Nudelman, Y.-Z. Lee, Y.-L. Hung, S. Kolusheva, A. Upcher, Y.-C. Chen, J.-Y. Chen, S.-C. Sue, R. Zarivach, *Front. Microbiol.* **2018**, 9, 2480.

[54] A. Arakaki, A. Yamagishi, A. Fukuyo, M. Tanaka, T. Matsunaga, *Mol. Microbiol.* **2014**, 93, 554.

[55] Y. Kanetsuki, M. Tanaka, T. Tanaka, T. Matsunaga, T. Yoshino, *Biochem. Biophys. Res. Commun.* **2012**, 426, 7.

[56] A. Komeili, Z. Li, D. K. Newman, G. J. Jensen, *Science* **2006**, 311, 242.

[57] O. Draper, M. E. Byrne, Z. Li, S. Keyhani, J. C. Barrozo, G. Jensen, A. Komeili, *Mol. Microbiol.* **2011**, 82, 342.

[58] A. Taoka, A. Kiyokawa, C. Uesugi, Y. Kikuchi, Z. Oestreicher, K. Morii, Y. Eguchi, Y. Fukumori, *mBio* **2017**, 8, e00679.

[59] D. Schultheiss, D. Schuler, *Arch. Microbiol.* **2003**, 179, 89.

[60] Y. Okamura, H. Takeyama, T. Sekine, T. Sakaguchi, A. T. Wahyudi, R. Sato, S. Kamiya, T. Matsunaga, *Appl. Environ. Microbiol.* **2003**, 69, 4274.

[61] S. Borg, J. Hofmann, A. Pollithy, C. Lang, D. Schuler, *Appl. Environ. Microbiol.* **2014**, 80, 2609.

[62] C. Lang, A. Pollithy, D. Schuler, *Appl. Environ. Microbiol.* **2009**, 75, 4206.

[63] T. Yoshino, T. Matsunaga, *Biochem. Biophys. Res. Commun.* **2005**, 338, 1678.

[64] S. Topp, C. M. Reynoso, J. C. Seeliger, I. S. Goldlust, S. K. Desai, D. Murat, A. Shen, A. W. Puri, A. Komeili, C. R. Bertozzi, *Appl. Environ. Microbiol.* **2010**, 76, 7881.

[65] T. Yoshino, A. Shimojo, Y. Maeda, T. Matsunaga, *Appl. Environ. Microbiol.* **2010**, 76, 1152.

[66] O. Raschdorf, J. M. Plitzko, D. Schuler, F. D. Muller, *Appl. Environ. Microbiol.* **2014**, 80, 4323.

[67] N. Philippe, L.-F. Wu, *J. Mol. Biol.* **2010**, 400, 309.

[68] O. Raschdorf, Y. Forstner, I. Kolinko, R. Uebe, J. M. Plitzko, D. Schüler, *PLoS Genet.* **2016**, 12.

[69] H. Chen, S.-D. Zhang, L. Chen, Y. Cai, W.-J. Zhang, T. Song, L.-F. Wu, *Front. Microbiol.* **2018**, 9, 1569.

[70] E. Cornejo, P. Subramanian, Z. Li, G. J. Jensen, A. Komeili, *mBio* **2016**, 7, e01898.

[71] A. Yamagishi, M. Tanaka, J. J. Lenders, J. Thiesbrummel, N. A. Sommerdijk, T. Matsunaga, A. Arakaki, *Sci. Rep.* **2016**, 6, 29785.

[72] A. Lohße, I. Kolinko, O. Raschdorf, R. Uebe, S. Borg, A. Brachmann, J. M. Plitzko, R. Müller, Y. Zhang, D. Schüler, *Appl. Environ. Microbiol.* **2016**, 82, 3032.

[73] U. Heyen, D. Schuler, *Appl. Microbiol. Biotechnol.* **2003**, 61, 536.

[74] R. P. Blakemore, D. Maratea, R. S. Wolfe, *J. Bacteriol.* **1979**, 140, 720.

[75] T. Tanaka, K. Kawasaki, S. Daimon, W. Kitagawa, K. Yamamoto, H. Tamaki, M. Tanaka, C. H. Nakatsu, Y. Kamagata, *Appl. Environ. Microbiol.* **2014**, 80, 7659.

[76] K. Kawasaki, Y. Kamagata, *Appl. Environ. Microbiol.* **2017**, 83.

[77] A. Komeili, H. Vali, T. J. Beveridge, D. K. Newman, *Proc. Natl. Acad. Sci. U. S. A.* **2004**, 101, 3839.

[78] A. Olszewska-Widdrat, G. Schiro, V. E. Reichel, D. Faivre, *Front. Microbiol.* **2019**, 10, 582.

[79] Y. A. Gorby, T. J. Beveridge, R. P. Blakemore, *J. Bacteriol.* **1988**, 170, 834.

[80] O. Raschdorf, D. Schuler, R. Uebe, *Methods Mol. Biol.* **2018**, 1841, 45.

[81] F. Guo, Y. Liu, Y. Chen, T. Tang, W. Jiang, Y. Li, J. Li, *Appl. Microbiol. Biotechnol.* **2011**, 90, 1277.

[82] E. Alphandery, S. Faure, O. Seksek, F. Guyot, I. Chebbi, *ACS Nano* **2011**, 5, 6279.

[83] L. Xiang, J. Wei, S. Jianbo, W. Guili, G. Feng, L. Ying, *Lett. Appl. Microbiol.* **2007**, 45, 75.

[84] T. Matsunaga, C. Nakamura, J. G. Burgess, K. Sode, *J. Bacteriol.* **1992**, 174, 2748.

[85] Registry of Standard Biological Parts, https://parts.igem.org/, accessed: 6/6, 2020.

[86] H. M. Salis, E. A. Mirsky, C. A. Voigt, *Nat. Biotechnol.* **2009**, 27, 946.

[87] I. Farasat, M. Kushwaha, J. Collens, M. Easterbrook, M. Guido, H. M. Salis, *Mol. Syst. Biol.* **2014**, 10, 731.

[88] C. Y. Ng, I. Farasat, C. D. Maranas, H. M. Salis, *Metab. Eng.* **2015**, 29, 86.

[89] Y. J. Chen, P. Liu, A. A. Nielsen, J. A. Brophy, K. Clancy, T. Peterson, C. A. Voigt, *Nat. Methods* **2013**, 10, 659.

[90] C. Lou, B. Stanton, Y. J. Chen, B. Munsky, C. A. Voigt, *Nat. Biotechnol.* **2012**, 30, 1137.

[91] J. R. Sadler, H. Sasmor, J. L. Betz, *Proc. Natl. Acad. Sci. U. S. A.* **1983**, 80, 6785.

[92] A. J. Meyer, T. H. Segall-Shapiro, E. Glassey, J. Zhang, C. A. Voigt, *Nat. Chem. Biol.* **2019**, 15, 196.

[93] M. H. Ryu, J. Zhang, T. Toth, D. Khokhani, B. A. Geddes, F. Mus, A. Garcia-Costas, J. W. Peters, P. S. Poole, J. M. Ane, C. A. Voigt, *Nat. Microbiol.* **2020**, 5, 314.

[94] Z. Oestreicher, E. Mumper, C. Gassman, D. A. Bazylinski, S. K. Lower, B. H. Lower, *J. Mater. Res.* **2016**, 31, 527.

[95] T. Yoshino, T. Matsunaga, *Appl. Environ. Microbiol.* **2006**, 72, 465.

[96] C. Lang, D. Schüler, *Appl. Environ. Microbiol.* **2008**, 74, 4944.

[97] N. Kroger, N. Poulsen, *Annu. Rev. Genet.* **2008**, 42, 83.

[98] N. Kroger, R. Deutzmann, M. Sumper, *Science* **1999**, 286, 1129.

[99] A. K. Wallace, N. Chanut, C. A. Voigt, *Adv. Funct. Mater.* **2020**, 2000849.

[100] E. L. Buckle, J. Sampath, N. Michael, S. D. Whedon, C. J. Leonen, J. Pfaendtner, G. P. Drobny, C. Chatterjee, *ChemBioChem* **2020**.

[101] S. L. Sewell, D. W. Wright, *Chem. Mater.* **2006**, 18, 3108.

[102] A. Tay, C. Murray, D. Di Carlo, *Adv. Funct. Mater.* **2017**, 27, 1703106.

[103] H. V. Nguyen, E. Suzuki, Z. Oestreicher, H. Minamide, H. Endoh, Y. Fukumori, A. Taoka, *Biochem. Biophys. Rep.* **2016**, 7, 39.

[104] Y. Zhang, X. Zhang, W. Jiang, Y. Li, J. Li, *Appl. Environ. Microbiol.* **2011**, 77, 5851.

[105] I. Ali, C. Peng, Z. M. Khan, I. Naz, *J. Basic Microbiol.* **2017**, 57, 643.

[106] D. Faivre, A. Olszewska-WIddrat, G. Schiro, V. Reichel, *Front. Microbiol.* **2019**, 10, 582.

[107] T. Prozorov, T. Perez-Gonzalez, C. Valverde-Tercedor, C. Jimenez-Lopez, A. Yebra-Rodriguez, A. Körnig, D. Faivre, S. K. Mallapragada, P. A. Howse, D. A. Bazylinski, *Eur. J. Mineral.* **2014**, 26, 457.

[108] S. Staniland, W. Williams, N. Telling, G. Van Der Laan, A. Harrison, B. Ward, *Nat. Nanotechnol.* **2008**, 3, 158.

[109] J. Li, N. Menguy, M.-A. Arrio, P. Sainctavit, A. Juhin, Y. Wang, H. Chen, O. Bunau, E. Otero, P. Ohresser, *J. R. Soc. Interface* **2016**, 13, 20160355.

[110] M. Tanaka, R. Brown, N. Hondow, A. Arakaki, T. Matsunaga, S. Staniland, *J. Mater. Chem.* **2012**, 22, 11919.

[111] H. Shimoshige, Y. Nakajima, H. Kobayashi, K. Yanagisawa, Y. Nagaoka, S. Shimamura, T. Mizuki, A. Inoue, T. Maekawa, *PLOS ONE* **2017**, 12.

[112] I. Kolinko, A. Lohße, S. Borg, O. Raschdorf, C. Jogler, Q. Tu, M. Pósfai, É. Tompa, J. M. Plitzko, A. Brachmann, *Nat. Nanotechnol.* **2014**, 9, 193.

[113] Y. Choi, T. J. Park, D. C. Lee, S. Y. Lee, *Proc. Natl. Acad. Sci.* **2018**, 115, 5944.

[114] B. D. Reiss, C. Mao, D. J. Solis, K. S. Ryan, T. Thomson, A. M. Belcher, *Nano Lett.* **2004**, 4, 1127.

[115] T. W. Giessen, P. A. Silver, *ACS Synth. Biol.* **2016**, 5, 1497.

[116] X. Liu, P. A. Lopez, T. W. Giessen, M. Giles, J. C. Way, P. A. Silver, *Sci. Rep.* **2016**, 6, 38019.

[117] M. E. Kovach, P. H. Elzer, D. S. Hill, G. T. Robertson, M. A. Farris, R. M. Roop, 2nd, K. M. Peterson, *Gene* **1995**, 166, 175.

[118] R. M. Shanks, N. C. Caiazza, S. M. Hinsa, C. M. Toutain, G. A. O'Toole, *Appl. Environ. Microbiol.* **2006**, 72, 5027.

[119] Y. Liu, G. R. Li, F. F. Guo, W. Jiang, Y. Li, L. J. Li, *Microb. Cell Fact.* **2010**, 9, 99.

[120] D. Schüler, R. Uhl, E. Bäuerlein, *FEMS Microbiol. Lett.* **1995**, 132, 139.

Figure captions and Tables

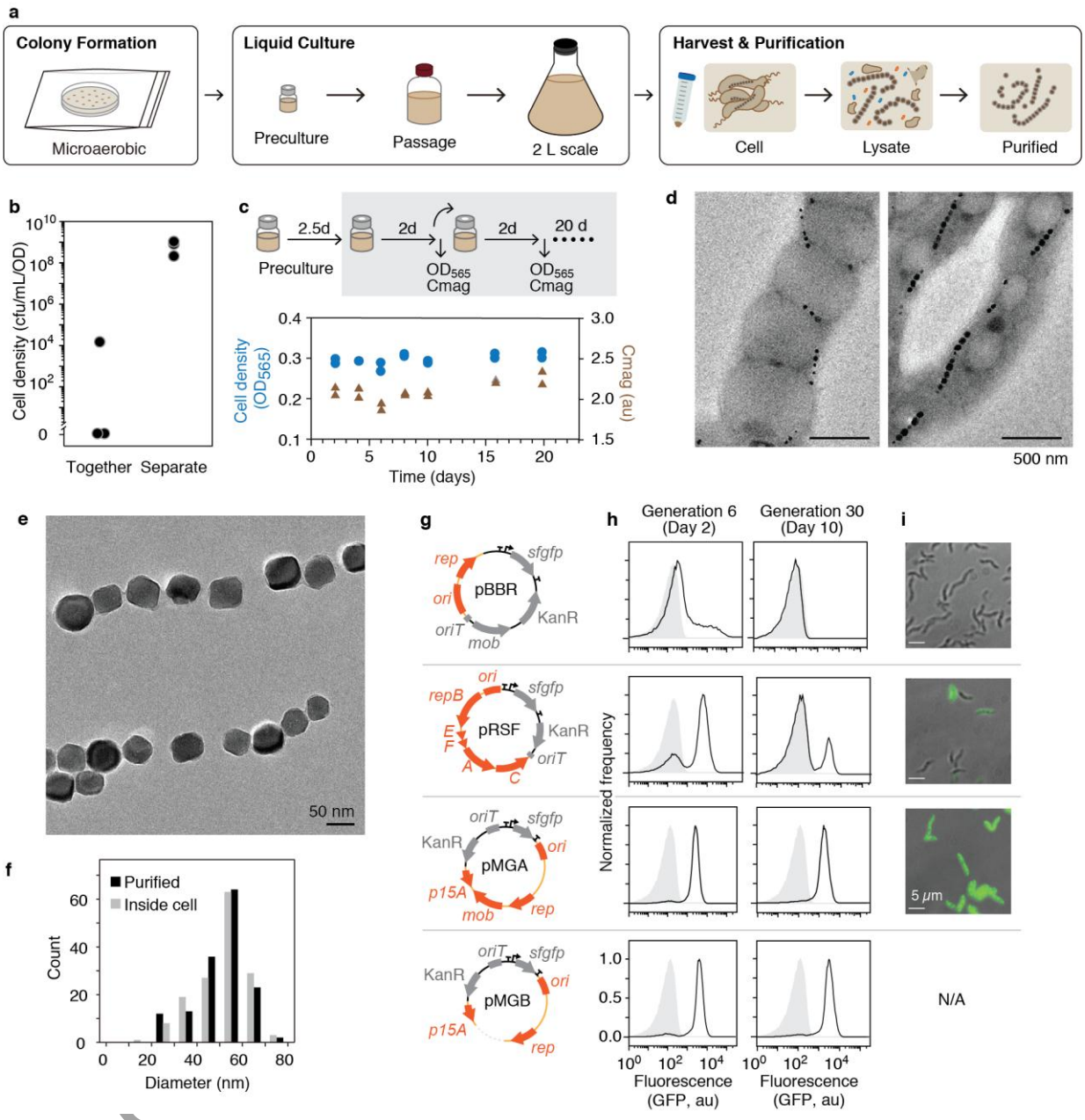

Figure 1: Optimization of magnetic nanoparticle production. (a) Culturing *M. magneticum* and subsequent purification steps for magnetosome production are shown. The full protocol is provided in the Methods and Supplementary Note 1. **(b)** The impact on cell growth of preparing agar plates by autoclaving the agar together versus separate from the mMSGM media is shown. The data represent three experiments performed on different days. **(c)** Cultures were passaged every 2 days up to 30 days. The cell density (OD_{565}) and magnetism (C_{mag}) were measured right before inoculation

into fresh media (Supplementary Figure 1f). The experiments were performed in duplicate, shown as the pairs of points. **(d)** Representative TEM image of *M. magneticum* cells cultured before (left) and after (right) optimization (Methods). The white globules are PHA. These experiments were performed on three different days with similar results. **(e)** Representative TEM image of the purified magnetosome nanoparticles after optimizing growing conditions. These experiments were performed on more than three different days with similar results. **(f)** Size comparison of purified magnetosomes with those quantified from cell images (Methods). The distribution of the magnetosomes inside the cells was quantified from randomly-selected 150 particles (19 cells). The distribution of the purified magnetosomes was obtained using 150 randomly-selected particles. **(g)** Plasmid maps; full sequences provided in Supplemental Table 4. Genes responsible for plasmid replication are shown in orange. **(h)** Plasmid stability. Cytometry distributions comparing cells with the plasmid expressing sfGFP (black) with cell autofluorescence (grey). These experiments were performed on two different days with similar results. **(i)** Fluorescence microscopy of images at Day 10. These experiments were performed on three different days with similar results.

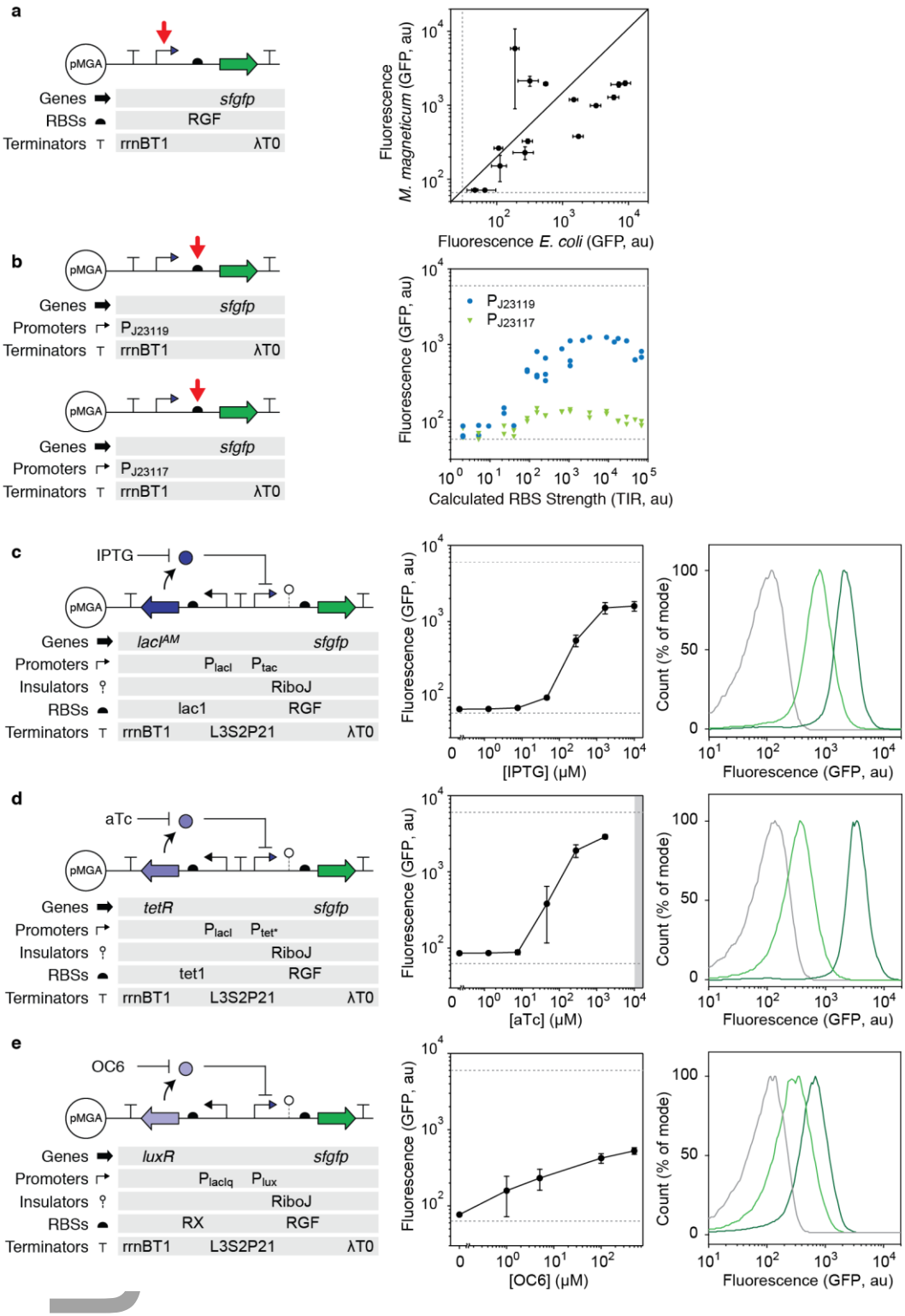

Figure 2: **Control of gene expression in *M. magneticum*.** Genetic part sequences are provided in Supplementary Table 1 and part strengths are provided in Table 1. **(a)** Characterization of constitutive promoters. The genetic system used to characterize expression is shown; the promoter

varied is marked with a red arrow. The right plot compares the promoter strengths when the same expression cassette is evaluated in *E. coli* (Methods). The dashed lines mark the autofluorescences of *M. magneticum* and *E. coli* without plasmid. **(b)** Characterization of RBSs. The genetic constructs are shown for measuring the strength of a RBS library (red arrows) when transcribed from two constitutive promoters of different strengths. Data are shown for three experiments performed on different days. **(c – e)** Inducible genetic systems in *M. magneticum* with circuit diagrams (left), dosage-dependent curves (middle) and cytometry (right). In all of dosage-dependent curves, the top dashed lines indicate the maximum expression level in *M. magneticum* (with the P_{rrn34} promoter in **a**), while the line on the bottom dashed lines indicates the autofluorescences of *M. magneticum* without a plasmid. **(c)** The IPTG sensor. The cytometry distributions are for (left to right): 0, 5 mM, 200 μM IPTG. **(d)** The aTc sensor. Grey shading indicates that cells did not grow. The cytometry distributions are for (left to right): 0, 40 μM, 1 mM aTc. **(e)** The OC6 sensor. The cytometry distributions are for (left to right): 0, 5 μM, 500 μM OC6. All of the points in response functions were calculated based on the mean of three experiments performed on different days and the error bars are the standard deviation.

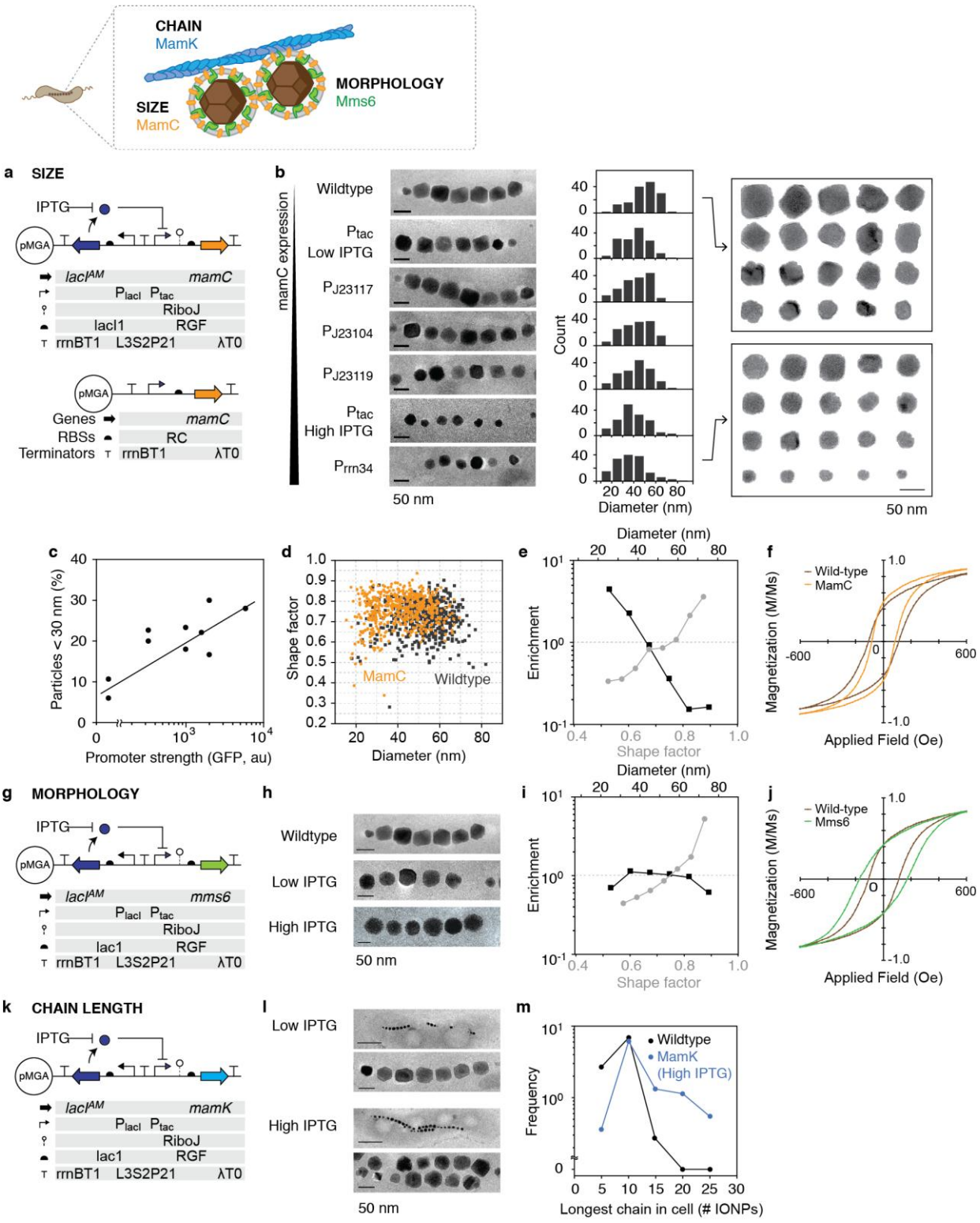

Figure 3: MAI gene overexpression and impact on IONP size and shape. The impacts of overexpressing additional genes and operons are provided in Supplementary Figures 8-27. **(a)** The genetic circuit diagrams to control *mamC* expression are shown: the top is an inducible system and

the bottom is under constitutive control. Genetic part sequences are provided in Supplemental Table 1. **(b)** The data are ordered by the strength of the promoter used to control *mamC* expression (Table 1). Representative TEM images of individual cells are shown (wider views of more cells are provided in Supplementary Figures 8 and 26). The size histograms were constructed based on *N* = 150 particles randomly selected from two cultures performed on different days. Right, twenty random particles are shown for the distributions with the largest and smallest averages, sampled from ~500 purified magnetosome particle images from a single culture. The larger TEM images are shown in Supplementary Figures 28 and 29. **(c)** The percent of the particles in the superparamagnetic size regime are plotted versus various promoters (based on strength) (Table 1) controlling *mamC*. The pairs of points represent two experiments performed on different days and particles obtained randomly from the two resulting TEM images. **(d)** The size and shape factor of *N* = 500 purified magnetosomes from wild-type or strain harboring P_{rrn34}-*mamC* from a single large-scale culture. The TEM images of the particle used for analysis are shown in Supplementary Figures 28 and 29. **(e)** The enrichments in magnetosome properties are shown for the data in part d for particles from cells overexpressing *mamC* divided by those obtained from the wild-type. The data are binned by 10 nm for diameter and 0.05 for shape factor, and the enrichment were calculated by dividing the value from particles produced by P_{rrn34}-*mamC* to that measured from particles produced by the wild-type. The dashed line indicates no over- or under-enrichment. **(f)** Magnetization hysteresis curve of wild-type and MamC magnetosomes. **(g)** The genetic construct for *mms6* expression is shown. **(h)** Representative TEM images of magnetosomes inside cells under low (0.1 mM) or high (1 mM) IPTG concentration compared to that of wildt-ype. These images are representative samples from Supplementary Figure 23. **(i)** The enrichment of magnetosome properties from *mms6*-overexpressing cells compared to those produced by the wild-type. See part e for how enrichment is calculated. The TEM images of the particle used for analysis are shown in Supplementary Figures 28 and 30. **(j)** Magnetization hysteresis curve of wild-type and Mms6 magnetosomes. **(k)** The genetic construct for controlling *mamK* expression is shown. **(l)** Representative TEM image of the cells induced by low (0.1 mM) or high (1 mM) IPTG concentration. The images were taken from those shown in Supplementary Figure 27. **(m)** Histogram of maximum numbers of magnetosomes in one chain. The data were collected from the TEM images of 48 and 32 *mamK* and wild-type cells, respectively, from three experiments performed on different days.

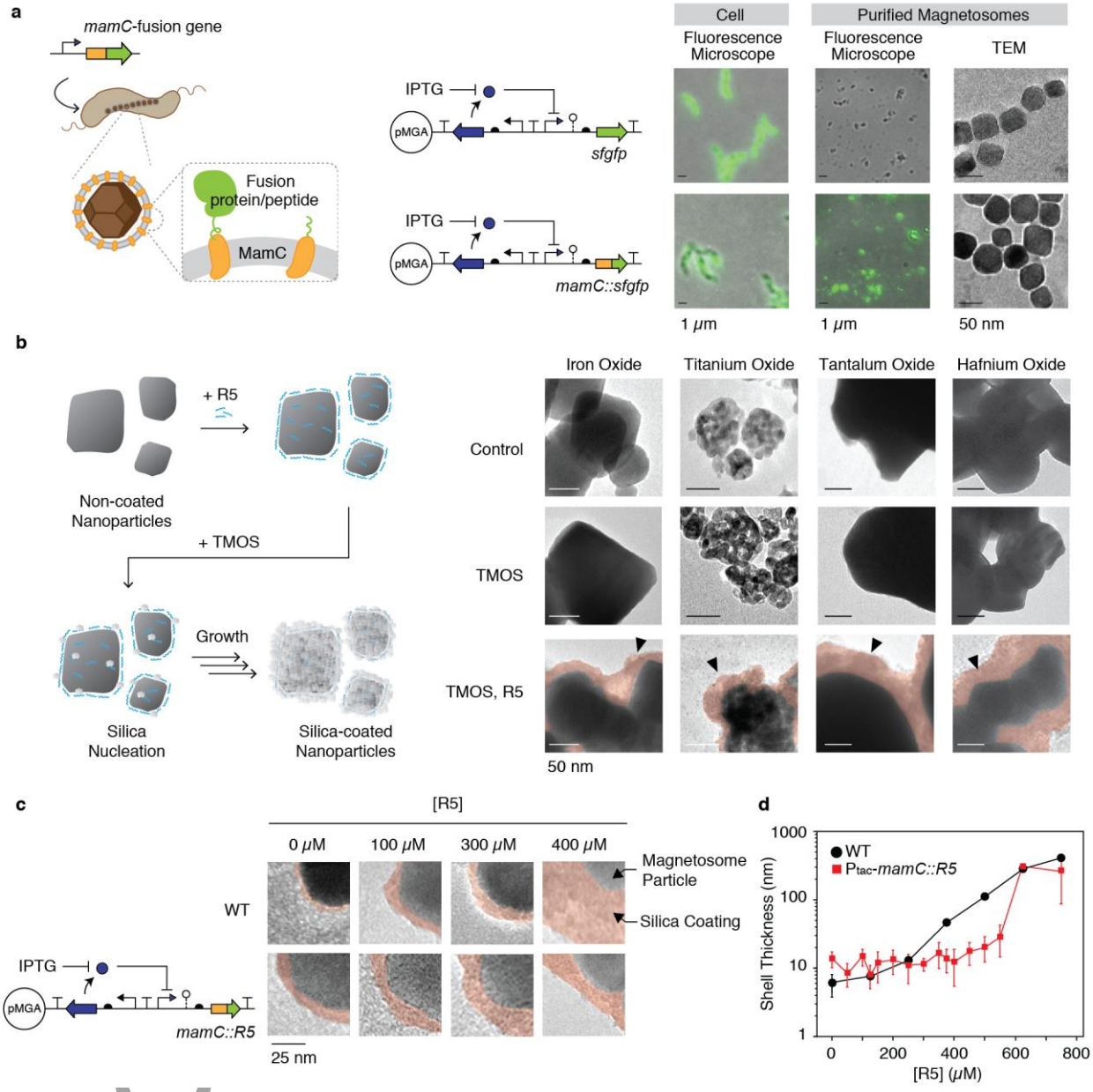

Figure 4: **Modification of magnetosome surfaces. (a)** Using the IPTG-inducible system, the expression and localization of sfGFP is compared to the MamC::sfGFP fusion. These experiments were performed on three days with similar results. **(b)** A schematic of the addition of R5 peptide to metal nanoparticles to nucleate a silica shell is shown. The silica shells can be seen with the addition of both 250 μM R5 and 1M TMOS (triangles and false-colored red). These experiments were performed on three days with similar results. **(c)** TEM images of silica-coated magnetosomes, either wild type displaying MamC::R5 (1 mM IPTG). These experiment were performed on three days with similar results. **(d)** Silica-shell thickness as a function of R5 concentration. Six TEM images were taken for each condition replicate and every particle with a distinguishable silica coating was measured.

For each condition replicate, 20 – 90 measurements were taken perpendicular to the nanoparticle surface, where a clear distinction could be deduced between the nanoparticle surface and the silica shell. Each point indicates the average from three experiments performed on different days and the error bars are the standard deviations.

Table 1: Genetic parts to control expression

Promoters		
Part name	DNA Sequence[a]	Strength
BBa_J23119	**TTGACA**GCTAGCTCAGTCCTAGG**TATAAT**GCTAGC	2000
BBa_J23111	**TTGACG**GCTAGCTCAGTCCTAGG**TATAGT**GCTAGC	1280
BBa_J23104	**TTGACA**GCTAGCTCAGTCCTAGG**TATTGT**GCTAGC	990
BBa_J23107	**TTTACG**GCTAGCTCAGTCCTAGG**TATTAT**GCTAGC	380
BBa_J23117	**TTGACA**GCTAGCTCAGTCCTAGG**GATTGT**GCTAGC	330
P_{tac}	**TTGACA**ATTAATCATCGGCTCG**TATAAT**GTTAGC	1900
P_{rrn1}	**TTGACA**GGGTCGGATGGGGCGGG**TAGAAC**CCGCCT	2300
P_{rrn1*}	**TTGACA**GCTAGCTCAGTCCTAGG**TAGAAC**GCTAGC	1200
P_{rrn34}	CGGGATTTGCCTTCGGGTAAAAACAGTGG**TTGACA**GGGTCGGA TGGGGCGAG**TAAAAC**CCGCCCCTCGCTGCGACGGACCGAAAGG GACGGGGCGGCAAAAAGGACCGGGTCAACGGTTTCCGCCTCCG GGCGAAAATGAAGTG**TTGACA**AGGATTTACGGGTCGGG**TAGAA A**CCGGCCTCCCCGCTGCGGCGGGGCCTTCGCCGAGACGAAGGA TCGGAGATCGGAAACGGTTTCCTGCTGTTT	5900
RBSs	DNA Sequence[b]	Strength[c]
Library	AAAGTCA**MMS**AGA**W**CAAGATAAA**S**G**S**G**S**TA**R**AAC	
R01	AAAGTCACCGAGAACAAGATAAACGCGCTAGAAC	70
R02	AAAGTCACCGAGAACAAGATAAACGCGCTAAAAC	70
R03	AAAGTCACCGAGATCAAGATAAACGCGCTAAAAC	80
R04	AAAGTCACCGAGAACAAGATAAACGGGCTAGAAC	130
R05	AAAGTCACCGAGAACAAGATAAACGGGGTAGAAC	80
R06	AAAGTCACCGAGATCAAGATAAACGCGGTAGAAC	460

R07	AAAGTCACCGAGAACAAGATAAAGGCGCTAAAAC	520
R08	AAAGTCACCGAGATCAAGATAAACGGGGTAGAAC	530
R09	AAAGTCACCGAGATCAAGATAAAGGGGCTAGAAC	870
R10	AAAGTCACCGAGAACAAGATAAAGGCGGTAGAAC	750
R11	AAAGTCACCGAGATCAAGATAAAGGGGCTAAAAC	1100
R12	AAAGTCACCGAGAACAAGATAAAGGGGGTAGAAC	1240
R13	AAAGTCACCGAGAACAAGATAAAGGGGGTAAAAC	1240
R14	AAAGTCACCGAGATCAAGATAAAGGGGGTAAAAC	1110
R15	AAAGTCAAAGAGATCAAGATAAAGGGGGTAAAAC	620
R16	AAAGTCAAACAGAACAAGATAAAGGGGGTAAAAC	740

a) Nucleotides that differ from the BBa_J23119 promoter are shown in yellow. The -35 and -10 regions are shown in bold. The nucleotides different from Prrn1 in the sequence are indicated in green. The -35/-10 sequence of Prrn1 and the spacer sequence of BBa_ promoter (indicated in orange) are used to construct a synthetic promoter.

b) The degenerate nucleotides are shown in boldface. M represents A or C; S represents C or G; W represents A or T; R represents A or G.

c) The value corresponds to that of J23119.

TOC summary

Magnetospirillum magneticum builds uniform Fe_3O_4 iron oxide nanoparticles (IONPs) with shapes and crystal forms difficult to achieve with chemical synthesis. Here, we have demonstrated a genetic control of IONP properties by controlling expression of *M. magneticum* genes that affect IONP properties, including size, morphology, chain length, and surface coating.